Tuning the laser-induced ultrafast demagnetization of transition metals

W. Töws and G. M. Pastor
Institut für Theoretische Physik, Universität Kassel, Heinrich-Plett-Straße 40, 34132 Kassel, Germany

(Received 20 September 2017; revised manuscript received 14 June 2019; published 1 July 2019)

The ultrafast demagnetization (UFD) dynamics of itinerant ferromagnets is theoretically investigated as a function of the characteristics of the initial laser excitation. A many-body *pd*-band Hamiltonian is considered which takes into account hybridizations, Coulomb interactions, spin-orbit interactions, and the coupling to the laser field on the same electronic level. In this way, a fruitful connection is established between the nonadiabatic quantum dynamics and the well-known equilibrium statistical mechanics of itinerant-electron ferromagnets. The time evolution during and after the pulse absorption is determined exactly by performing numerical Lanczos propagations on a small cluster model with parameters appropriate for Ni. The most relevant laser parameters, namely, the fluence F, wave length λ, polarization $\hat{\varepsilon}$, and pulse duration τ_p are varied systematically. The results show how F, $\hat{\varepsilon}$, and τ_p allow one to control the total absorbed energy, the spectral distribution of the initial excitation, and the subsequent magnetization dynamics. The calculations show that reasonable changes in these parameters do not affect the UFD dynamics qualitatively and have only a minor influence on the timescale $\tau_{\rm dm}$ which characterizes the initial demagnetization. In contrast, our model predicts that the degree of demagnetization $\Delta S_z/S_z^0$ achieved for $t \gtrsim \tau_{\rm dm}$ correlates well with the average number of electrons excited by the laser or average number of absorbed photons $n_{\rm ph}$, which can be tuned by varying the fluence, spectral distribution and polarization of the laser pulse. The theoretical results are discussed by comparing them with available experiments. From a fundamental perspective, the robustness of the ultrafast demagnetization effect is theoretically demonstrated, as a phenomenon reflecting the intrinsic dynamics of the metallic 3*d* valence electrons. A wide variety of well-focused possibilities of tailoring the efficacy of the ultrafast demagnetization process is thereby opened.

DOI: 10.1103/PhysRevB.100.024402

I. INTRODUCTION

Over the past twenty years, a wide range of different time-resolved experiments have demonstrated that the excitation of magnetic transition metals (TMs) and rare earths with short laser pulses triggers an ultrafast demagnetization (UFD) of the material on a subpicosecond or picosecond timescale [1–16]. This remarkable effect offers new possibilities of ultrafast control and manipulation of the magnetization, which could find multiple applications in spin-electronic devices and storage media. Understanding the nontrivial quantum physics behind this phenomenon is obviously crucial for any knowledge-oriented material design. Therefore several mechanisms explaining the UFD have been proposed in the literature [13–45]. On the one hand, one finds models in which the central role is played by the coupling between the narrow-band electrons responsible for magnetism and some distinct, a priori nonmagnetic degrees of freedom or field. In this context, let us mention the mechanisms based on electron-phonon spin-flip scattering [14,23–29], on the transport of spin-polarized electrons [30–37], and on the coherent relativistic interaction between the photon field and the electronic spins [38–40]. On the other hand, two purely electronic theories have also been proposed, in which the essential part of the demagnetization takes place within the electronic system, as a result of the coupling between the spin and translational degrees of freedom in the presence of the lattice potential [41–45]. To this category belong the time-dependent density-functional studies reported in Refs. [41–44]. These explain the UFD as a throughout breakdown of the spin density and local magnetic moments in all unit cells, which involves spin-orbit driven spin flips and spin currents. An alternative approach, which is particularly relevant for the present paper, is the many-body electronic model Hamiltonian proposed in Ref. [45]. In this case, the experimentally observed demagnetization is explained as the consequence of an ultrafast breakdown of the FM correlations between the local 3*d* magnetic moments which remain highly stable at all times. From the latter investigations the following microscopic picture of the magnetization dynamics emerges [45]: (i) at the start, the laser excitation changes the occupation of the valence-electron states by inducing mainly 3*d*-to-4*p* electronic transitions, thus creating holes in the magnetically relevant 3*d* band. During this process the total magnetization of the sample remains essentially unchanged, since spin is conserved in optical transitions. (ii) These changes in occupations trigger the dynamics by opening so far Pauli-blocked new channels for spin-orbit coupling (SOC) induced local angular-momentum transfers, dominantly from the atomic d-electron spins $\vec{s}_i$ to the d-orbital moments $\vec{l}_i$. Taking into account that the local spin moments are initially large and the orbital moments almost quenched, this process alone would tend to enhance $\langle \vec{l}_i \rangle$ at the expense of $\langle \vec{s}_i \rangle$, since the total local angular momentum $\vec{j}_i = \vec{l}_i + \vec{s}_i$ is conserved by the SOC. (iii) However, the perpetual motion of electrons in the lattice

due to interatomic hopping quenches most efficiently any incipient increase of the average orbital angular momentum $\langle\vec{L}\rangle = \sum_i \langle\vec{l}_i\rangle$ on a timescale of the order of one femtosecond. The result of these three simple fundamental processes is the rapid decrease of the average electronic angular momentum $\langle\vec{J}\rangle = \sum_i \langle\vec{j}_i\rangle$ and magnetization of the sample as a function of time. The demagnetization occurs essentially at the same rate as the spin-to-orbital angular momentum transfer, which is governed by the SOC and thus corresponds to a characteristic demagnetization time $\tau_{\rm dm}$ of the order of 100 fs. Notice, moreover, that the sum of the angular momenta associated to the electronic and ionic degrees of freedom is strictly preserved by the electron-lattice interactions. Therefore the decrease of $\langle\vec{J}\rangle$ is exactly compensated by an increase of the lattice angular momentum $\vec{L}_{\rm lat}$, occurring at the same rate. The fact that high local-moment stability, electron delocalization, and spin-orbit interactions are all inherent features of itinerant-electron magnetism explains the experimentally observed universality of the UFD effect. Further details on the electronic mechanism of UFD are discussed in Ref. [45].

In past years, a considerable research activity has been focused on the role of the initial excitation in the UFD process, and on the possibilities of controlling the spin dynamics by tuning the laser-pulse characteristics [42,46–48]. For example, it has been recently demonstrated that the degree of demagnetization can in principle be controlled by changing the shape and spectral distribution of the pump pulse [42]. It is therefore most interesting to correlate the degree of demagnetization with the material parameters and electronic structure. Furthermore, one would like to understand how the efficiency of the demagnetization process depends on the degree of excitation of the ferromagnet. Varying the intensity of the pumping pulse at a given frequency allows us to adjust the number of absorbed photons, excited electrons and absorbed energy. Changing the laser frequency for a given absorbed energy one should be able to discern the role of the number of excitations, and thus gain further insight into thermalization effects. In addition, one may also consider different circularly and linearly polarized light, in order to explore how an initial transfer of angular momentum upon laser absorption may affect the subsequent dynamics. Finally, adjusting the laser-pulse duration τ_p, from ultrashort highly intense excitations to values of τ_p comparable with SOC relaxation time, should help us to reveal any specific spin dynamics taking place while the laser field is active, and which may result from SOC-laser interference effects [38–40]. It is the purpose of this paper to investigate the role of the initial laser excitation on the magnetization dynamics of ferromagnetic TMs and to quantify the possibilities of tuning the ultrafast demagnetization by its means. To this aim, we consider a many-body electronic theory in which the dynamics of the electronic translational, orbital and spin degrees of freedom, as well as their coupling to the external electric field, are described quantum mechanically and on the same footing [45].

The remainder of the paper is organized as follows. The theoretical background, including a derivation of the model Hamiltonian, the involved approximations, and the parameters used for the calculations, is presented in Sec. II. Exact numerical results for the magnetization dynamics as a function of the fluence, wave length, polarization and duration of the laser pulse are presented and discussed in Sec. III. Finally, Sec. IV summarizes the main conclusions and perspectives.

II. THEORETICAL BACKGROUND

In the following, we first derive the electronic model [45] used in the present investigations of the laser-induced magnetization dynamics by explicitly pointing out all the involved approximations. The complete many-body problem, which includes both electronic and ionic degrees of freedom, is simplified by using the *Born-Oppenheimer* approximation, which decouples the electronic and ionic dynamics [49]. This is justified, as usual, by the large ion-to-electron mass ratio, and the resulting differences in the corresponding timescales. Since we are interested in the dynamics of the magnetization, which is given by the spin and orbital electronic contributions, we focus on the electronic degrees of freedom so that the ion coordinates appear only as parameters of the quantum many-electron problem. Although the lattice dynamics is ignored in all the calculations reported in Sec. III, we shall return to it at the end of this section and in Sec. IV, when discussing the conservation of total (lattice plus electron) angular momentum and the possible role of the coupling to phonons.

The spin and orbital magnetic moments of transition metals are known to be dominated by the $3d$-electron contributions. Moreover, the prime optical excitations of the $3d$ states, which result from the pumping laser, involve transitions to the nearby $4p$ orbitals. Therefore, in order to capture the main physics of laser-excited $3d$ electrons in ferromagnetic TMs, it is reasonable to concentrate on the correlated-electron dynamics within these two bands. The corresponding many-body pd Hamiltonian is given by

$$\hat{H} = \hat{H}_0 + \hat{H}_C + \hat{H}_{\rm SO} + \hat{H}_E(t)\,, \tag{1}$$

where

$$\hat{H}_0 = \sum_{i\alpha\sigma} \varepsilon_\alpha\, \hat{n}_{i\alpha\sigma} + \sum_{ij}\sum_{\alpha\beta\sigma} t_{ij}^{\alpha\beta}\, \hat{c}^\dagger_{i\alpha\sigma}\hat{c}_{j\beta\sigma} \tag{2}$$

describes the single-particle electronic structure of the $3d$ and $4p$ bands. In the usual notation, $\hat{c}^\dagger_{i\alpha\sigma}$ ($\hat{c}_{i\alpha\sigma}$) creates (annihilates) an electron at atom i with radial and orbital quantum numbers $\alpha = nlm$ and spin σ (nl refers to $3d$ and $4p$). The corresponding electron number operator is $\hat{n}_{i\alpha\sigma}$. For simplicity, the energy levels ε_α of the atomic-like $3d$ and $4p$ orbitals $|\varphi_{i\alpha}\rangle$ are assumed to be independent of m. The interatomic hopping integrals $t_{ij}^{\alpha\beta}$ describe the delocalization of the electrons throughout the lattice. Formally, they are given by $t_{ij}^{\alpha\beta} = \langle\varphi_{i\alpha}|(-\hbar^2\nabla^2/2\mu + \phi^{\rm lat})|\varphi_{j\beta}\rangle$, where μ stands for the electron mass and $\phi^{\rm lat}$ for the effective lattice potential, which depends on all atomic positions $\vec{R}_i$. Notice that the hoppings $t_{ij}^{\alpha\beta}$, but also the energy levels $\varepsilon_\alpha = t_{ii}^{\alpha\alpha}$, incorporate the leading contribution to the electron dynamics resulting from the electron-lattice interaction as given by $\phi^{\rm lat}$. In the following, the hopping integrals $t_{ij}^{\alpha\beta}$ are determined by using the two-center approximation, which takes into account the most important terms in $\phi^{\rm lat}$ due to the ions i and j [50]. In this case, $t_{ij}^{\alpha\beta}$ depends only on the relative vector $\vec{R}_{ij} = \vec{R}_i - \vec{R}_j$, as well as on the radial and orbital quantum numbers nlm of the

orbitals α and β. Further details on the calculation of $t_{ij}^{\alpha\beta}$ may be found in Appendix A.

The second term, $\hat{H}_C$ in Eq. (1), refers to the electron-electron interaction. For simplicity, we approximate it by taking into account only the dominant intra-atomic terms among the $3d$ electrons, which are known to be responsible for the magnetic behavior of TMs. Starting from the general intra-atomic expression

$$\hat{H}_C = \frac{1}{2}\sum_i \sum_{\alpha\beta\gamma\delta\in 3d} \sum_{\sigma\sigma'} V_{\alpha\beta\gamma\delta}\, \hat{c}^\dagger_{i\alpha\sigma}\, \hat{c}^\dagger_{i\beta\sigma'}\, \hat{c}_{i\delta\sigma'}\, \hat{c}_{i\gamma\sigma}\,, \quad (3)$$

we consider only the largest two-orbital integrals, namely, the direct terms $U_{\alpha\beta} = V_{\alpha\beta\alpha\beta}$ and the exchange terms $J_{\alpha\beta} = V_{\alpha\beta\beta\alpha}$ ($\alpha \neq \beta$), which are the most important for the magnetic behavior. Moreover, the orbital dependencies of $U_{\alpha\beta}$ and $J_{\alpha\beta}$ are neglected by setting them equal to their average values $U_{\alpha\beta} = U$ and $J_{\alpha\beta} = J$. While the orbital dependencies of the intra-atomic d-electron repulsions are known to be important for a quantitative description of orbital magnetism [51], they are not essential for describing the total spin polarization within the $3d$ band, even as a function of temperature [52]. Taking into account these simplifications one obtains the particularly transparent form [52–55]

$$\hat{H}_C = \frac{1}{2}\left(U - \frac{J}{2}\right)\sum_i \hat{n}_i^d\left(\hat{n}_i^d - 1\right) - J\sum_i \hat{\vec{s}}_i^d \cdot \hat{\vec{s}}_i^d + \frac{J}{2}\sum_{i\alpha\in 3d} \hat{n}_{i\alpha}(2 - \hat{n}_{i\alpha}) + \frac{J}{4}\sum_i \hat{n}_i^d. \quad (4)$$

Here, $\hat{n}_i^d = \sum_{\alpha\in 3d,\sigma} \hat{n}_{i\alpha\sigma}$ denotes the operator for the total number of $3d$ electrons at atom i, $\hat{\vec{s}}_i^\alpha$ ($\hat{n}_{i\alpha}$) is the spin (number) operator for the orbital α at atom i, and $\hat{\vec{s}}_i^d = \sum_{\alpha\in 3d} \hat{\vec{s}}_i^\alpha$ the total $3d$-electron spin operator at atom i. The first terms, proportional to the number of pairs of d electrons, take into account the changes in the Coulomb energy resulting from charge fluctuations. Although important for correlations, they have a visibly nonmagnetic character. The second terms, proportional to $(\hat{\vec{s}}_i^d)^2$, favor a parallel alignment of all the $3d$ spins at each atom (Hund's first rule). They are responsible for the formation and strong stability of the local spin moments ($J \sim 1$ eV). Part of the energy gain upon local moment formation (33%–50% depending on the number of unpaired electrons) is compensated by the third terms, which are proportional to $\hat{n}_{i\alpha}(2 - \hat{n}_{i\alpha})$. These terms are actually ignored in the subsequent dynamics, since their contribution results in an effective reduction of the exchange integral J, and since they are unaffected by the relative orientation of the unpaired spins. Finally, the last terms amount to an unimportant constant energy shift which can be incorporated in the definition of the bare levels ε_{3d} [see Eq. (2)].

For the sake of compactness, it is useful to define a new direct Coulomb repulsion parameter U as the average repulsion $U - J/2$ between d electrons having parallel and antiparallel spins. In this way one obtains the model interaction in its final form [45]

$$\hat{H}_C = \frac{U}{2}\sum_i \hat{n}_i^d\left(\hat{n}_i^d - 1\right) - J\sum_i \hat{\vec{s}}_i^{\,d} \cdot \hat{\vec{s}}_i^{\,d}. \quad (5)$$

Notice that $\hat{H}_C$, as the full Coulomb interaction, conserves both the spin $\vec{s}_i^{\,d}$ and orbital $\vec{l}_i$ angular momenta of the atoms, since the rotational invariance of the *first-principles* interaction is not altered by the local approximations. In this context it is useful to recall that this model has been successfully applied in numerous previous studies of the equilibrium ground-state and finite-temperature properties of transition-metal magnetism [56].

The third term in Eq. (1) is the spin-orbit coupling operator

$$\hat{H}_{\rm SO} = \xi \sum_i \sum_{\alpha\alpha'\in 3d} \sum_{\sigma\sigma'} (\vec{l}\cdot\vec{s})_{\alpha\sigma,\alpha'\sigma'}\, \hat{c}^\dagger_{i\alpha\sigma}\hat{c}_{i\alpha'\sigma'} \quad (6)$$

in an intra-atomic approximation within the $3d$ band, where the parameter ξ denotes the SOC strength. The matrix elements $(\vec{l}\cdot\vec{s})_{\alpha\sigma,\alpha'\sigma'}$ of $\hat{\vec{l}}_i \cdot \hat{\vec{s}}_i$ at atom i couple the spin and orbital degrees of freedom, thereby conserving the total local angular momentum $\vec{j}_i = \vec{l}_i + \vec{s}_i$.

The last term $\hat{H}_E$ in Eq. (1) introduces the interaction with the external laser field, which is treated in the intra-atomic dipole approximation. For linearly polarized light, we have

$$\hat{H}_E(t) = e\hat{\vec{r}}\cdot\vec{E}(t) = e|\vec{E}(t)| \sum_{i\alpha\beta\sigma} \langle\alpha|\hat{\varepsilon}\cdot\hat{\vec{r}}|\beta\rangle\, \hat{c}^\dagger_{i\alpha\sigma}\hat{c}_{i\beta\sigma}\,, \quad (7)$$

where $\vec{E}(t)$ refers to the uniform classical electric field, $\hat{\varepsilon}$ denotes a dimensionless normalized polarization vector, and $e > 0$ is the electron charge. In the case of circularly polarized laser pulses $\hat{H}_E$ is replaced by the operator $\hat{H}_E^\sigma$, which describes an electric field with helicity $\sigma = \pm 1$ carrying an angular momentum $\sigma\hbar$ along the z axis. This is given by

$$\hat{H}_E^\pm(t) = e|\vec{E}(t)|\, \hat{P}_p\, (\hat{\varepsilon}_\pm \cdot \hat{\vec{r}})\, \hat{P}_d + \text{H.c.}\,, \quad (8)$$

where $\hat{P}_d$ ($\hat{P}_p$) denotes the projection operator onto the $3d$ ($4p$) orbitals and $\hat{\varepsilon}_\pm = (\hat{e}_x \pm i\hat{e}_y)/\sqrt{2}$ is the complex polarization vector. As usual, $\hat{e}_x$ and $\hat{e}_y$ stand for the unit vectors along the x and y axis. Since the dipole matrix elements $\langle\alpha|\hat{\vec{r}}|\beta\rangle$ satisfy the atomic selection rule $\langle nlm|\hat{\vec{r}}|n'l'm'\rangle = 0$ unless $l - l' = \pm 1$, the optical excitation involves only $3d$-$4p$ transitions. A more detailed account of the dipole matrix elements is given in Appendix B. The operator $\hat{H}_E^+$ can be interpreted as follows. The first term in Eq. (8) describes the absorption of a photon which transfers an angular momentum $+\hbar$ to a $3d$ electron making a transition to a $4p$ orbital ($m \to m + 1$). Hermiticity, as ensured by the second term in Eq. (8), implies the emission of a photon with angular momentum $\hbar$ in the reverse electronic transition from a $4p$ to a $3d$ orbital ($m \to m - 1$). Analogously, the operator $\hat{H}_E^-$ with the opposite helicity $\sigma = -1$ describes the absorption (emission) of an angular momentum $-\hbar$ in the optical transitions from $3d$ to $4p$ ($4p$ to $3d$) orbitals.

Before closing the discussion of the model, it is worth recalling that the field-free Hamiltonian $\hat{H} = \hat{H}_0 + \hat{H}_C + \hat{H}_{\rm SO}$ represents a purely electronic model, which describes the dynamics of electrons within the lattice potential $\phi^{\rm lat}$ generated by the ions at given fixed positions $\vec{R}_j$. Since $\phi^{\rm lat}$ is obviously not isotropic, the electronic angular momentum $\vec{L} + \vec{S}$ is not conserved, where $\vec{L} = \sum_i \vec{l}_i$ ($\vec{S} = \sum_i \vec{s}_i$) stands for the total electronic orbital (spin) angular momentum. However, the combined system of electrons and ions represents a closed

and therefore rotationally invariant system. Consequently, it is clear that the total angular momentum of electrons and ions $\vec{J} = \vec{L} + \vec{S} + \vec{L}^{\text{lat}}$ remains a formally rigorous constant of motion, where $\vec{L}^{\text{lat}}$ denotes the angular momentum of the lattice. An explicit account of the time dependence of the lattice angular momentum would require to consider the dynamics of the ionic degrees of freedom, which is beyond the scope of the present work.

Model simplifications and parameters

In order to achieve an exact numerical solution of the many-body dynamics without involving often hardly controllable and symmetry breaking mean-field approximations, we keep the *pd*-band model as transparent as possible by introducing two simplifications. First, we reduce the orbital degeneracy by considering only the $3d$ orbitals having $|m| \leqslant 1$ and the $4p$ orbital having $m = 0$. This approximation reduces the numerical effort involved in the exact numerical propagation without significantly affecting the $3d$-$4p$ optical absorption process, the electronic delocalization and exchange interactions responsible for magnetism, or the angular-momentum transfer between spin and orbital degrees of freedom induced by the SOC. Similar reductions of the local orbital degeneracy have often been used in the context of electron correlations and itinerant magnetism, in particular, in connection with the Hubbard model [57–59].

The second approximation consists in performing the numerical propagations on a small cluster model. In this work, we consider equilateral triangles ($N_a = 3$ atoms) having $N_e = 4$, 5, and 7 electrons, and an equilateral $N_a = 4$ rhombus with $N_e = 5$, where the length of the short diagonal equals the side length. This allows us to explore various geometries and band fillings having different electronic structures. As shown in Sec. III, the small-cluster approximation can be justified *a posteriori* by the local character of the mechanism responsible for angular momentum transfer and ultrafast demagnetization. However, it also brings some limitations, such as the discreteness of the energy spectrum, a significant underestimation of the d-band width, and the impossibility of describing long-range electron correlations, the consequences of which need to be discussed.

The model parameters are specified as follows. The hopping integrals $t_{jk}^{\alpha\beta}$ are determined by considering nearest-neighbor (NN) Slater-Koster integrals $(dd\sigma) = 0.6$ eV, $(dd\pi) = -0.3$ eV, $(pp\sigma) = 1.5$ eV, and $(pd\sigma) = -0.4$ eV. The absolute values of these parameters are similar to those obtained by fitting the band structure of bulk Ni [60,61] or in canonical transition-metal bands [62,63]. Notice that the pp hoppings are significantly larger than the dd ones, which corresponds to a rather broad sp-band and a narrow $3d$-band, as found in $3d$ TMs such as Ni. Moreover, the NN pd hoppings are important, almost of the same order of magnitude as the difference between the $4p$ and the $3d$ energy levels $\varepsilon_p - \varepsilon_d = 1.4$ eV. This leads to a significant pd hybridization and a small but not negligible p-level ground-state occupation, which is consistent with the spd hybridization found in $3d$ TMs.

The largest energy scale is given by the direct Coulomb integral $U = 8.0$ eV, a value taken from experimental photoemission spectra and theoretical calculations of the Ni density of electron states [64–67]. The intra-atomic exchange integral J yields stable FM ground states whose easy magnetization direction defines the z axis. For the rhombus having $N_a = 4$ atoms and $N_e = 5$ electrons, we use $J = 1.5$ eV and obtain a ground-state off-plane spin polarization $S_z^0 = 2.15\,\hbar$. For the triangular clusters having $N_e = 4$, 5, and 7, we use $J = 0.8$–1.0 eV. The ground states of the $N_e = 4$ and 5 triangles exhibit off-plane easy magnetization axes and spin polarizations of $S_z^0 = 1.96\,\hbar$ and $S_z^0 = 1.34\,\hbar$, while the ground state of the $N_e = 7$ triangle exhibits an in-plane easy magnetization plane and $S_z^0 = 1.52\,\hbar$.

The smallest energy scale in the model is the spin-orbit coupling strength $\xi = -80$ meV. Typical values for $3d$ TMs are in the range $|\xi| = 50$–100 meV [68]. Notice that the sign of ξ has been changed for systems having a less than half-filled d band, in order to reproduce the parallel alignment between $\vec{L}$ and $\vec{S}$ found in Ni, Co, and Fe [69]. This corresponds to performing the electron-hole transformation $\hat{h}_{i\alpha\sigma} = \hat{c}^{\dagger}_{i\alpha\sigma}$, which does not affect the Coulomb interaction and only changes the sign of the hopping integrals. Explicit calculations show that changing the sign of ξ does not affect the time dependence of the discussed observables in any significant way. However, as discussed in Sec. III, the value of $|\xi|$ and its relation to the other energy scales, in particular the d-band width, are important in order to determine the characteristic timescale of the magnetization dynamics.

The spin dynamics is triggered by an optical pump pulse having a Gaussian form

$$\vec{E}(t) = \hat{\varepsilon} \cdot E_0 \cos(\omega t) \exp\left(-t^2/\tau_p^2\right), \tag{9}$$

where $\omega = 2\pi c/\lambda$ is the laser frequency. The pulse, centered at $t = 0$, has a duration characterized by the pulse width τ_p. The intensity of the electric field can be measured by the maximal amplitude E_0 of $\vec{E}(t)$, which is related to the energy flow per unit area or fluence F: $E_0 = (2/\pi)^{1/4}\sqrt{2F/(c\varepsilon_0\tau_p)}$, where ε_0 is the vacuum permittivity. In order to investigate the role of the pump-pulse parameters in the laser-induced magnetization dynamics, we vary F, $\hat{\varepsilon}$ and τ_p systematically. In this way, we quantify the dependence of the spin relaxation on the initial laser excitation. In cases where F, τ_p or $\hat{\varepsilon}$ are not explicitly mentioned, we use $F = 40$ mJ/cm^2, $\tau_p = 5$ fs and a linear in-plane polarization $\hat{\varepsilon}$ along one NN bond in the triangle or along the long diagonal in the rhombus. These values correspond approximately to the typical numbers of excited electrons per atom observed in experiments [9]. It should be noted that the pump-pulse durations used in experiments ($\tau_p^{\text{exp}} \simeq 25$–$100$ fs) [9–16,35] are significantly larger than the $\tau_p = 5$ fs considered in the present study. From a theoretical perspective, short excitation pulses have the advantage of allowing a clear separation between the initial excitation and the subsequent magnetization dynamics. However, this choice also implies that the calculated demagnetization time is somewhat underestimated, since the energy is more rapidly absorbed. Finally, the strength of the coupling between the electronic degrees of freedom and $\vec{E}$ is characterized by the reduced matrix element $\langle 3d||\hat{T}^{(1)}||4p\rangle$ [see Eqs. (B5) and (B6) in Appendix B]. For the calculations, throughout this work, we set $\langle 3d||\hat{T}^{(1)}||4p\rangle = 0.5$ Å, which corresponds to the typical extension of $3d$ and $4s$ orbitals in $3d$ TMs. The precise value of $\langle 3d||\hat{T}^{(1)}||4p\rangle$ is not important for our conclusions.

In the following section, we investigate the consequences of the laser excitation on the FM ground state $|\Psi_0\rangle$ by propagating $|\Psi(t)\rangle$ numerically under the action of the time-dependent electric field. The time evolution is calculated by using the short-time iterative Lanczos propagation method [70]. Once the many-body wave function $|\Psi(t)\rangle$ is obtained we compute the expectation values $O(t) = \langle\Psi(t)|\hat{O}|\Psi(t)\rangle$ of the observables $\hat{O}$ of physical interest, for example, the total spin magnetization $\hat{S}_z$, the local spin and orbital moments $\hat{\vec{s}}_i$ and $\hat{\vec{l}}_i$, and the spin-correlation functions $\hat{\vec{s}}_i \cdot \hat{\vec{s}}_j$.

III. RESULTS AND DISCUSSION

Before solving and analyzing the dynamics it is important to keep in mind that the hybridizations due to the electron-lattice interaction, the Coulomb interactions and the laser-absorption processes, which are described by $\hat{H}_0$, $\hat{H}_C$, and $\hat{H}_E$, all conserve the total spin $\vec{S} = \sum_i \vec{s}_i$, i.e., $[\hat{H}_0, \hat{\vec{S}}] = [\hat{H}_C, \hat{\vec{S}}] = [\hat{H}_E, \hat{\vec{S}}] = 0$. The spin-rotational invariance is broken only by the SOC since $[\hat{H}_{\rm SO}, \hat{\vec{S}}] \neq 0$. However, the SOC operator $\hat{H}_{\rm SO}$ commutes with the sum $\hat{\vec{l}}_i + \hat{\vec{s}}_i$ of the local orbital and spin angular momenta at each TM atom. Therefore, any spin-flip process induced by SOC necessarily involves a local angular momentum transfer between $\vec{s}_i$ and $\vec{l}_i$, in which the sum $\vec{l}_i + \vec{s}_i$ is conserved. This local intra-atomic symmetry notwithstanding, neither the local orbital moment $\vec{l}_i$ nor the total orbital angular momentum $\vec{L} = \sum_i \vec{l}_i$ are conserved throughout the dynamics, since the lattice potential is not rotationally invariant (i.e., $[\hat{H}_0, \hat{\vec{l}}_i] \neq 0$ and $[\hat{H}_0, \hat{\vec{L}}] \neq 0$). This can be traced back to the fact that the interatomic hoppings $t_{ij}^{\alpha\beta}$ connect orbitals with different azimuthal quantum numbers m at different atoms. The previous fundamental symmetry considerations are essential for understanding the ultrafast magnetization dynamics from a microscopic quantum perspective. The use of time-dependent mean-field approximations to the dynamics seems very questionable in this context, because they artificially break the spin-rotational invariance with respect to $\hat{H}_0$, $\hat{H}_C$, and $\hat{H}_E$. In contrast, exact time propagations —although limited in their application to small finite systems—have the clear advantage of complying with all fundamental conservation laws. They should therefore allow us to derive rigorous conclusions [45].

The purpose of this Section is to investigate the dynamics of ferromagnetic TMs as a function of the laser fluence F, photon energy $\hbar\omega$, electric-field polarization $\hat{\varepsilon}$, and pulse duration τ_p, in order to quantify to what extent these experimentally tunable parameters can be used to taylor the magnetization dynamics. Results for different model systems and band fillings are contrasted. The correlations between degree of initial electronic excitation, absorbed energy, demagnetization time and degree of demagnetization are analyzed. General trends are inferred.

A. Laser fluence

The laser fluence F is naturally expected to play an important role in the subsequent spin relaxation since it controls the level of electronic excitation. In order to quantify its effect,

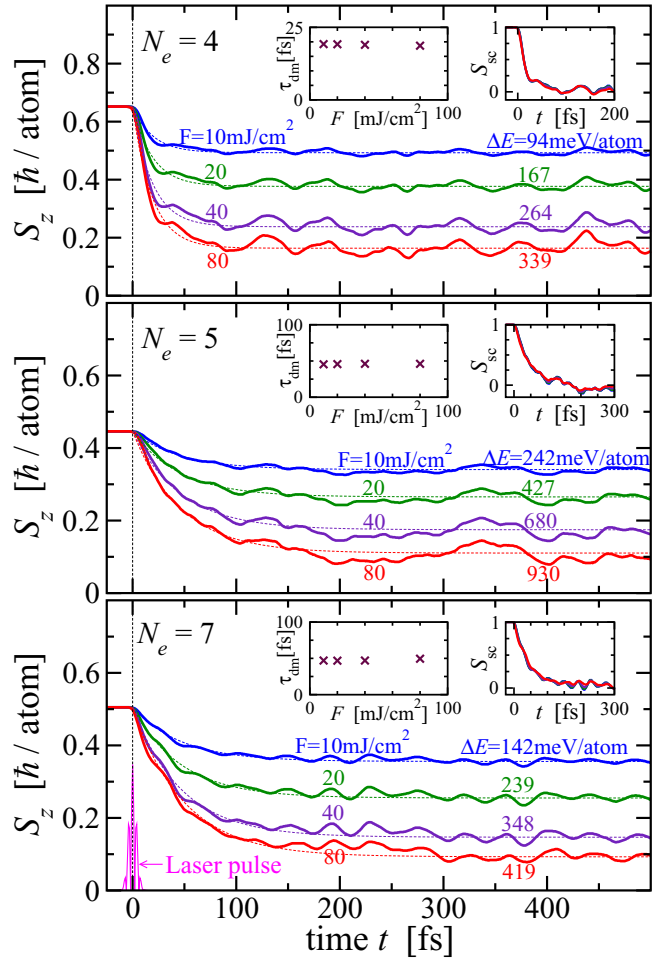

FIG. 1. Time dependence of the spin magnetization in an equilateral triangle with $N_e = 4$, 5, and 7 electrons, after excitation using a linearly polarized 5 fs laser pulse with wave length $\lambda = 1051$, 556, and 849 nm, respectively. The considered laser fluences F are indicated together with the corresponding absorbed energies per atom ΔE. The left insets show the demagnetization times $\tau_{\rm dm}$ as a function of F, as obtained from exponential fits to $S_z(t)$ given by the dashed curves in the main panels. The right insets show, for all considered values of F, the nearly identical time dependencies of the corresponding scaled spin magnetization $S_{\rm sc}(t) = [S_z(t) - S_z^\infty]/\Delta S_z$. In the bottom panel the amplitude $E(t)$ of the triggering electric field is illustrated.

we have determined the magnetization dynamics $S_z(t)$ for different representative values of F and for different structures and number of electrons N_e. This also gives us the opportunity to explore the dependence of the ultrafast demagnetization on band filling. Since the excitation spectrum depends on the precise structure and band filling of the model, and in order that the results can be compared, we have chosen the laser wave length such that it matches the absorption spectrum. The pulse shape is illustrated at the bottom panel of Fig. 1. The results of Figs. 1 and 2 show that similar laser-induced demagnetizations take place for all considered geometries and band fillings. One observes that $S_z(t)$ decreases rapidly after the pulse passage at $t = 0$ ($\tau_p = 5$ fs) reaching values close to the long-time limit S_z^∞ in about 100 fs. The

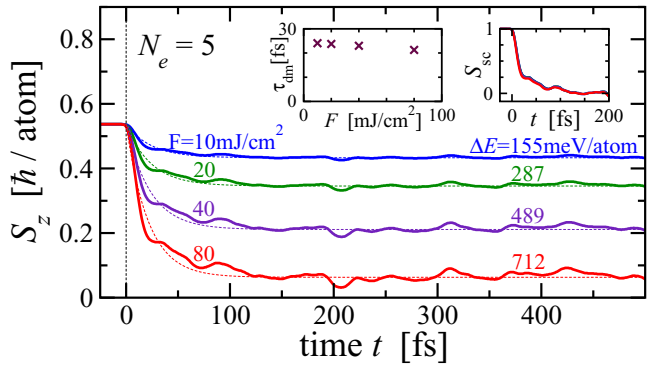

FIG. 2. Time dependence of the spin magnetization in a rhombus having $N_e = 5$ valence electrons. The excitation at $t = 0$ corresponds to a linearly polarized 5 fs laser pulse with wave length $\lambda = 385$ nm. See the caption of Fig. 1.

characteristic demagnetization timescale $\tau_{\rm dm}$ can be obtained by fitting an exponential law of the form $S_z(t) = S_z^\infty + [S_z(0) - S_z^\infty]\exp\{-t/\tau_{\rm dm}\}$ to the exact calculated numerical propagations, where $S_z(0)$ is the spin polarization at the time $t = 0$ when the electric field amplitude $E(t)$ reaches its maximum. Alternatively, one could set $S_z(0)$ equal to the ground-state magnetization, in which case one obtains a somewhat larger estimation of $\tau_{\rm dm}$.

From the fits, shown as thin dashed curves in the figures, one obtains $\tau_{\rm dm} \simeq 20$–50 fs depending on the structure (triangle or rhombus) and the number of electrons ($N_e = 4$–7). Notice that the spin relaxation occurs essentially after the passage of the laser pulse, since $\tau_{\rm dm}$ is always much larger than the considered pulse duration $\tau_p = 5$ fs. This implies that the demagnetization effect is not the direct result of the interaction with the laser electric field, but rather the consequence of an intrinsic process occurring within the excited electronic system. Indeed, previous studies show that the interplay between d-electron SOC, the associated spin-to-orbital angular momentum transfer, and the electronic motion in the lattice is at the origin of the ultrafast demagnetization [45]. The spin-orbit interactions acting on the excited electrons bring about a local flux of angular momentum from the atomic spins $\vec{s}_i$ to the atomic orbits $\vec{l}_i$ on a timescale of the order of $\hbar/\xi \simeq 10$ fs. At the same time, the electronic hoppings between different atoms quench any incipient increase of the total orbital angular momentum $\vec{L} = \sum_i \vec{l}_i$ on a very short timescale of only $\hbar/t_{jk}^{\alpha\beta} \simeq 1$ fs. This prevents any accumulation of the transfered spin angular momentum in the orbital degrees of freedom. The local character of the above discussed mechanism of angular momentum transfer, including the laser excitation dominated by intra-atomic dipole transitions, supports the physical validity of the present small-cluster exact-propagation approach (see Sec. II).

Before any further analysis of the role of the various laser parameters on the magnetization dynamics, it is important to point out that the values of the demagnetization times $\tau_{\rm dm} \simeq$ 20–50 fs obtained with the present model parameters and approximations are a factor 3–5 smaller than the typical values $\tau_{\rm dm}^{\rm exp} \simeq 120$–$160$ fs inferred from recent experiments on Ni [10,11,14]. The first and physically most relevant reason for the underestimation of $\tau_{\rm dm}$ is the small-cluster approximation, which underestimates the d-band width W_d and tends to overestimate the spin-to-orbital angular momentum transfer rate. The SOC parameter ξ defines the timescale $\hbar/\xi \simeq 10$ fs involved in SOC-induced spin flips. Since ξ is the smallest energy scale in the Hamiltonian, it leads to the slowest processes which control the changes in the spin polarization. However, in order to determine the actual rate of the SOC-induced angular momentum transfer (e.g., in the framework of perturbation theory [71]) it is equally important to take into account the average density of spin-flipped final states, which scales roughly proportional to the inverse d-band width $1/W_d$. In a small-cluster model, W_d is seriously underestimated and, therefore, the spin-to-orbital angular momentum transition rates are overestimated. In our case, using bulklike nearest-neighbor hopping integrals, we obtain a single-particle d-band width $W_d \simeq 2$ eV, which is almost a factor 3 smaller than the typical bulk value $W_d = 5$–6 eV. Representative calculations have been performed using larger hoppings and thus larger W_d in order to quantify this trend. They show indeed a corresponding increase of $\tau_{\rm dm}$ as the average number of d states per unit energy ($\sim 1/W_d$) decreases. For example, for $W_d =$ 6 eV, we obtain $\tau_{\rm dm} = 60$–150 fs. In addition, the discreteness of the energy spectrum and the spatial confinement of the cluster single-particle d states are also expected to result in an overestimation of the spin-orbit matrix elements. A second, less fundamental reason behind our underestimation of $\tau_{\rm dm}$ is the considered pulse duration $\tau_p = 5$ fs, which is significantly shorter than the typical experimental values $\tau_p^{\rm exp} \simeq 25$–$100$ fs [9–16,35]. This choice of τ_p is motivated by the interest of having a well-defined sharp excitation, which allows us to clearly discern between the absorption process and the subsequent magnetization dynamics. As discussed in Sec. III D, increasing the pulse duration increases $\tau_{\rm dm}$ since the energy is absorbed more slowly. Finally, one should take into account the role of the SOC constant ξ, which directly affects $\tau_{\rm dm}$. A systematic ensemble of calculations based on exact numerical time propagations shows that $\tau_{\rm dm}$ is approximately proportional to W_d/ξ^2, in qualitative agreement with the spin-orbit spin-flip rates estimated within first-order time-dependent perturbation theory [71]. This implies that small changes in ξ can have a significant impact on $\tau_{\rm dm}$. For example, using a somewhat smaller, though still reasonable value of $\xi = 50$ meV, and leaving all other model parameters as stated in Sec. II, we obtain $\tau_{\rm dm} \approx 80$ fs for the triangle with $N_e = 4$ electrons. In sum, taking into account our parameter choice and the approximations inherent to the small-cluster model used for the exact many-body time propagations, one concludes that the values of the demagnetization time $\tau_{\rm dm}$ reported in this paper, though smaller than the observed ones, are consistent with experiment [9–16,35].

Figures 1 and 2 clearly show that the larger F the larger the demagnetization $\Delta S_z = S_z^0 - S_z^\infty$, where S_z^0 denotes the initial spin polarization. For instance, in the triangle with $N_e = 7$ electrons the long-time spin polarization decreases from $S_z^\infty = 0.36\,\hbar$ to $S_z^\infty = 0.09\,\hbar$ per atom when the fluence is increased from $F = 10$ to 80 mJ/cm^2. However, the characteristic shape of $S_z(t)$, and in particular the demagnetization time $\tau_{\rm dm}$, depend weakly on F. To clarify this point, the insets in Figs. 1 and 2 show, on the right hand side, the scaled

spin magnetization $S_{sc}(t) = [S_z(t) - S_z^{\infty}]/\Delta S_z$ as a function of time t for all considered fluences F. In addition, on the left hand side, the demagnetization time τ_{dm} is given as a function of F. One observes that for all considered systems $S_{sc}(t)$ and τ_{dm} are essentially independent of F, i.e., of the degree of excitation (10 mJ/cm^2 $\leqslant F \leqslant$ 80 mJ/cm^2). However, τ_{dm} depends to some extent on the lattice structure and band filling, although it always remains in the range of a few tens of femtoseconds for $|\xi| = 80$ meV. This can be understood by recalling that the coupling between spin and translational degrees of freedom, which results from spin-orbit interactions, can be very sensitive to the details of the electronic structure. In fact, it is well-known that the magneto-crystalline anisotropy energy, easy magnetization axis, and orbital moments of transition-metal systems depend strongly on lattice structure and band filling [72–75]. Furthermore, notice that weak oscillations are superimposed to the general exponential decrease of the calculated $S_z(t)$. These become somewhat weaker (stronger) for shorter (longer) pulse durations τ_p, as the laser-field spectrum becomes broader (narrower) and the final excited state involves a larger (smaller) number of eigenfrequencies. They are possibly a consequence of the discreteness of the energy spectrum of the small cluster models used for the numerical time propagations.

It is instructive to compare our theoretical results for the fluence dependence of the UFD effect with available experiments [8,14]. The measurements on Ni by Koopmans *et al.* have shown that both the relative demagnetization ΔS_z and the demagnetization time τ_{dm} increase with increasing fluence [14]. While results for ΔS_z are in agreement with our trends, the results for τ_{dm} are not. However, more recent experiments on Ni by Tengdin *et al.* indicate a qualitatively different behavior, namely, an essentially fluence-independent demagnetization time [8], which coincides with the predictions of our model (see Figs. 1 and 2). In this context, it is interesting to observe that Tengdin *et al.* have fitted the time dependence of their magnetization data by using up to three distinct exponential functions: The first one describes the initial laser-triggered demagnetization, which is investigated in this paper, whereas the remaining ones correspond to the subsequent magnetization recovery. In this way, they were able to separate the timescale of the ultrafast demagnetization from the much slower magnetization recovery. In Ref. [14], the demagnetization time τ_{dm} has been obtained as the time at which the drop of the magnetization towards its lowest value is completed by 63%. Concerning the final recovery process, both experimental groups have clearly observed that it depends significantly on the fluence of the pumping laser. Therefore it is possible that the fluence dependence of $S_z(t)$, and the demagnetization time derived from it, are affected by the energy dissipation processes involved in the magnetization recovery, particularly as the level of excitation increases.

It is interesting to investigate the experimentally observed increase of the demagnetization ΔS_z with increasing fluence F by analyzing the spectral distribution of the many-body state $|\Psi(t)\rangle$ after the pump-pulse passage (e.g., $t \geqslant$ 15 fs for a 5 fs laser pulse). For this purpose, we expand $|\Psi\rangle = \sum_k \alpha_k |\psi_k\rangle$ in the stationary states $|\psi_k\rangle$ of the field-free Hamiltonian $\hat{H} = \hat{H}_0 + \hat{H}_C + \hat{H}_{SO}$ satisfying $\hat{H}|\psi_k\rangle = E_k|\psi_k\rangle$. The spectral distribution of $|\Psi\rangle$ is then given by

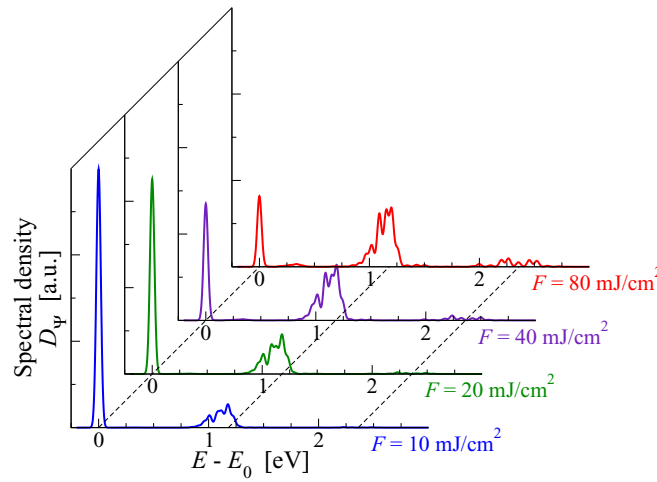

FIG. 3. Spectral density $D_\Psi(\epsilon)$ of the excited many-body state $|\Psi(t)\rangle$ after the laser-pulse passage ($t \geqslant$ 15 fs) as a function of excitation energy $\epsilon = E - E_0$. Results are given for the equilateral triangle having $N_e = 4$ and representative laser fluences F. The laser wave length is $\lambda = 1051$ nm ($\hbar\omega = 1.18$ eV). The discrete spectral lines have been broadened with a finite width $\delta = 20$ meV for the sake of clarity. The ground-state energy and the excitation energies corresponding to the absorption of one and two photons are indicated by the dashed lines.

$$D_\Psi(\epsilon) = \sum_k |\langle\psi_k|\Psi(t)\rangle|^2 \, \delta(\epsilon - \epsilon_k), \tag{10}$$

where $\epsilon = E - E_0$ is referred to the ground-state energy E_0 and $\epsilon_k = E_k - E_0$. Notice that $\hat{H}$ and thus the spectral distribution $D_\Psi(\epsilon)$ of $|\Psi(t)\rangle$ are independent of t once the pulse has passed (e.g., $t \geqslant 3\tau_p$). Figure 3 shows $D_\Psi(\epsilon)$ for a triangle with $N_e = 4$, which has been excited with a 5 fs laser pulse of wave length $\lambda = 1051$ nm ($\hbar\omega = 1.18$ eV) and fluences $F = 10$, 20, 40, and 80 mJ/cm^2. Three main peaks or groups of nearby peaks are distinguished around $\epsilon = 0$, $\hbar\omega$, and $2\hbar\omega$. They correspond to the ground state and to the absorption of 1 and 2 photons. One observes how the spectral weight of the excited-state manifolds around $\hbar\omega$ and $2\hbar\omega$ increases with increasing F at the expense of the ground-state contribution $|\langle\Psi_0|\Psi(t)\rangle|^2$. This reflects the growing level of electronic excitation and can be directly related to the degree of demagnetization $\Delta S_z/S_z^0 = (S_z^0 - S_z^{\infty})/S_z^0$ achieved at long times $t \gg \tau_{dm}$. Indeed, a simple argument allows us to approximately express $\Delta S_z/S_z^0$ in terms of the angle $\alpha = \arccos\langle\Psi_0|\Psi(t)\rangle$ between the excited state $|\Psi(t)\rangle$ at $t \geqslant 3\tau_p$ and the ground state $|\Psi_0\rangle$. Writing

$$|\Psi(t)\rangle = \cos(\alpha)\,|\Psi_0\rangle + \sin(\alpha)\,|\Delta\Psi(t)\rangle \tag{11}$$

with $\langle\Psi_0|\Delta\Psi(t)\rangle = 0$ and $\langle\Delta\Psi(t)|\Delta\Psi(t)\rangle = 1$ we have

$$S_z(t) = \cos^2(\alpha)\, S_z^0 + \sin^2(\alpha)\,\langle\Delta\Psi(t)|\hat{S}_z|\Delta\Psi(t)\rangle\,. \tag{12}$$

The demagnetization in the long-time limit is then given by

$$\Delta S_z = \sin^2(\alpha)\big[S_z^0 - S_z^*(\infty)\big], \tag{13}$$

where $S_z^*(t) = \langle\Delta\Psi(t)|\hat{S}_z|\Delta\Psi(t)\rangle$ is the magnetization in the excited states at time t. This shows that $\Delta S_z/S_z^0$ is proportional

to the spectral weight $\sin^2(\alpha)$ transferred to the excited states or, in other words, to the level of excitation. Since $S_z^*(0) \simeq S_z^0$ (i.e., essentially no change in the spin polarization occurs during the pulse passage) the proportionality factor $S_z^0 - S_z^*(\infty) = S_z^*(0) - S_z^*(\infty)$ gives a measure of the efficiency of the demagnetization in the excited-state manifolds. It is interesting to observe that the dynamics of the many-electron system yields a remarkably effective reduction of the excited-state magnetization $S_z^*(t)$. In fact, in some cases (e.g., a triangle having $N_e = 7$ electrons) the quenching of $S_z^*(t)$ is nearly complete [i.e., $S_z^*(\infty) \simeq 0$]. While it is tempting to interpret this in terms of the statistical hypothesis of equal a priori probability, there are many examples where no full excited-state quenching is found. For instance, in a triangle having $N_e = 4$ or 5 electrons, as well as the rhombus, one finds that $S_z^*(\infty)$ is significantly larger than zero [$S_z^*(\infty) \simeq 0.06 - 0.13\,\hbar$ per atom, see Sec. III B].

At this stage, one may wonder whether the relation between the degree of long-time demagnetization and the level of excitation is not simply a consequence of the fact that with increasing fluence F and increasing $\sin^2(\alpha)$ also the absorbed energy ΔE increases. In order to clarify this matter, it is important to investigate the dynamical magnetic response as a function of the photon energy $\hbar\omega$.

B. Absorbed energy versus average number of absorbed photons

The preceding section has shown that the main consequence of increasing the level of electronic excitation is to enhance the degree of demagnetization $\Delta S_z = S_z^0 - S_z^\infty$ at long times, at least for the considered range of fluence F. A complementary way of investigating the dependence of ultrafast demagnetization on the level of excitation and on the absorbed energy ΔE is to vary systematically the photon energy $\hbar\omega$. In this way, the importance of the absorbed energy and of the average number of electrons excited by the laser or of absorbed photons $n_{\rm ph} = \Delta E/\hbar\omega$ can be tell apart.

In the following, different laser frequencies are considered, for which the absorption probabilities are significant. The corresponding exact time dependences of $|\Psi(t)\rangle$ and $S_z(t)$ have been numerically determined. In all cases, the UFD effect is observed with demagnetization times $\tau_{\rm dm} = 18$–62 fs for the triangle with $N_e = 4$ electrons, $\tau_{\rm dm} = 23$–62 fs for the triangle with $N_e = 5$, $\tau_{\rm dm} = 42$–122 fs for the triangle with $N_e = 7$, and $\tau_{\rm dm} = 15$–86 fs for the rhombus with $N_e = 5$. This confirms that the UFD effect is an intrinsic characteristic of the correlated electronic system, which is qualitatively independent of the details of the triggering excitation. Nevertheless, notice that the precise value of $\tau_{\rm dm}$ depends to some extent on the laser frequency ω. This shows that different optical absorptions lead to different excited states, or more generally, different spectral distributions $D_\Psi(\epsilon)$, which exhibit their own specific many-body dynamics. Incidentally, this may also indirectly cause a fluence dependence of $\tau_{\rm dm}$. Assuming a rapid thermalization of the electronic translational degrees of freedom after the laser absorption, one expects that the distribution of the excited many-body states should become broader as the fluence F increases. This would render higher excitation energies accessible and could thus result in changes in $\tau_{\rm dm}$ as a function of F. Unfortunately, this hypothesis cannot be quantified numerically in the present framework, since the cluster models accessible to exact time propagations are too small to allow a true thermalization or self-averaging [76].

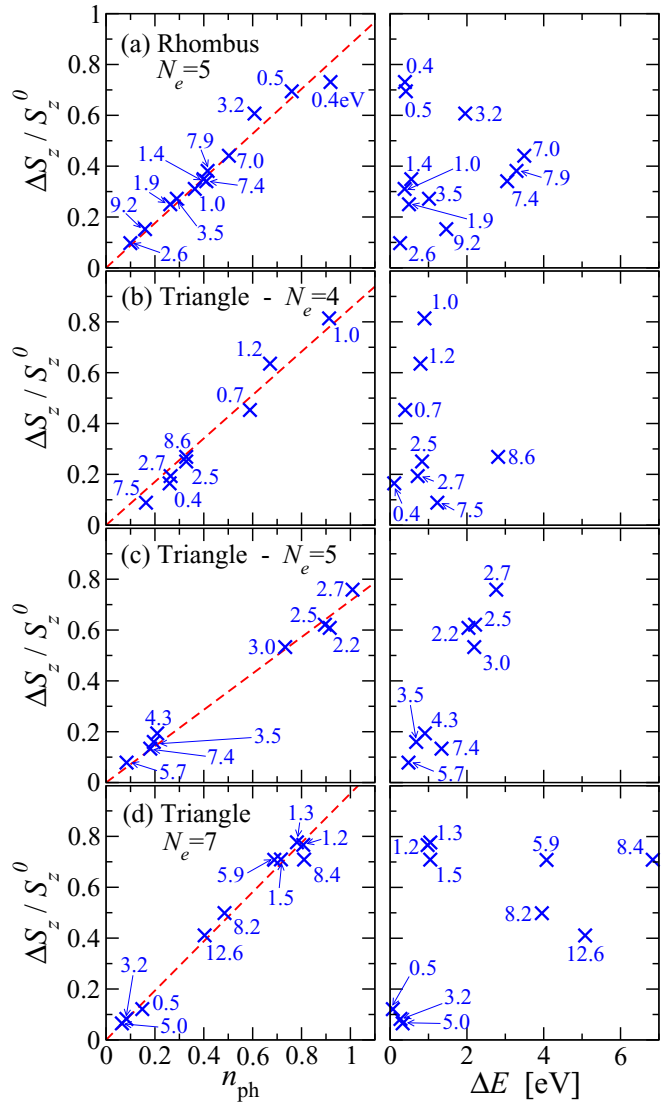

FIG. 4. Correlation between the laser-induced degree of demagnetization $\Delta S_z/S_z^0$ at long times $t \gg \tau_{\rm dm}$ and the absorbed energy ΔE (right) or the average number of absorbed photons $n_{\rm ph} = \Delta E/\hbar\omega$ (left), where ω is the angular frequency of the exciting laser. The crosses are obtained from the exact calculated time evolution for (a) a rhombus with $N_e = 5$ electrons, and an equilateral triangle having (b) $N_e = 4$, (c) 5, and (d) 7 electrons. The laser fluence is always $F = 40\,{\rm mJ/cm^2}$, while the different photon energies $\hbar\omega$ are indicated in eV. The dashed straight lines on the left panels are fits to the approximate linear dependence of $\Delta S_z/S_z^0$ on $n_{\rm ph}$.

The long-time limit of the demagnetization $\Delta S_z = S_z^0 - S_z^\infty$ has been derived for each $\hbar\omega$ from the numerical time propagations. The thus obtained relative demagnetizations $\Delta S_z/S_z^0$ are shown in Fig. 4 as a function of the absorbed energy ΔE (right-hand side) and of the average number of absorbed photons $n_{\rm ph} = \Delta E/\hbar\omega$ (left-hand side). The scatter plot on the right-hand side of Fig. 4 is so disperse that no

relation between ΔE and $\Delta S_z/S_z^0$ can be established. ΔS_z is obviously not a function of ΔE alone. In contrast, the left-hand side figure reveals a remarkably simple, approximately linear dependence of $\Delta S_z/S_z^0$ on $n_{\rm ph}$. For example, in the triangle with $N_e = 7$, $\Delta S_z/S_z^0$ are nearly the same for $\hbar\omega = 1.5$ eV and $\hbar\omega = 5.9$ eV although the absorbed energies $\Delta E = 1.0$ and 4.1 eV differ widely by a factor four. The corresponding $n_{\rm ph} = 0.72$ and 0.69 are very similar. In other cases, for example in the triangle with $N_e = 4$, the absorbed energies are very similar ($\Delta E = 0.9$ eV for $\hbar\omega = 1.0$ eV and $\Delta E = 0.8$ eV for $\hbar\omega = 2.5$ eV) but the relative demagnetizations differ widely ($\Delta S_z/S_z^0 = 0.81$ and 0.25, respectively). One concludes that the average number of absorbed photons $n_{\rm ph}$, or equivalently, the number of single-particle electronic excitations induced by the pumping pulse, rather than the absorbed energy, determines primarily the strength of the demagnetization. This is consistent with the discussion at the end of Sec. III A showing that $\Delta S_z/S_z^0$ is proportional to the spectral weight transfered to the excited states during the laser-pulse absorption.

The slope γ of the linear dependence $\Delta S_z/S_z^0 \simeq \gamma\, n_{\rm ph}$ can be related to the efficiency of the demagnetization in the excited states $S_z^*(\infty)$, which was introduced at the end of the Sec. III A. Assuming for simplicity that only the ground state and the lowest excited states around $\hbar\omega$ contribute to the spectral distribution of $|\Psi(t)\rangle$ after the pump pulse, one can easily show that $\sin^2(\alpha)$ in Eqs. (11)–(13) is equal to the average number of absorbed photons $n_{\rm ph} = \Delta E/\hbar\omega$. Therefore $\gamma = [S_z^0 - S_z^*(\infty)]/S_z^0$ represents the relative demagnetization efficiency in the excited states. Figure 4 (left) shows that γ and thus $S_z^*(\infty)$ do not depend significantly on $\hbar\omega$. However, they depend somewhat on the considered cluster model and band filling. For example, for the triangle with $N_e = 4$ and 5 electrons, and for the rhombus with $N_e = 5$ electrons we find $\gamma \simeq 0.72 - 0.88 < 1$. This implies that the magnetic order in the excited states $|\Delta\Psi\rangle$ is not fully destroyed as a result of the many-electron dynamics. In other words, $|\Delta\Psi\rangle$ remains ferromagnetic to a small extent even at very long times. In contrast, for the triangle with $N_e = 7$, the FM correlations in $|\Delta\Psi\rangle$ are fully lost along the dynamics. The demagnetization of $|\Delta\Psi\rangle$ is in this case almost complete, namely, $S_z^*(\infty)/S_z^0 \simeq 0.03$ or $\gamma \simeq 0.97$.

According to our exact model calculations, the energy per atom ΔE, which is absorbed during the pump pulse, does not give the appropriate measure of the degree of excitation of the electronic system in relation to subsequent $\Delta S_z/S_z^0$. This is physically interesting, since it contrasts with the idea that the translational degrees of freedom of the electronic system should rapidly thermalize in a spin-conserving way. Indeed, if the latter were so, the energy absorbed in any field-induced single-particle transition would be rapidly redistributed among the electrons, thus erasing any memory of the details of the triggering excitation (e.g., the number of initial single-particle transitions or number of absorbed photons). Let us recall that the characteristic times involved in electron-lattice and electron-electron interactions ($\hbar/t_{ij}^{\alpha\beta}$ and $\hbar/U$) are at least an order of magnitude shorter than the typical spin-orbit and demagnetization times. All these short-time dynamical processes are properly taken into account in our studies. Still, it is also true that our calculations are unable to describe the approach to thermal equilibrium, since the exact time propagations are performed for closed purely electronic systems (Neumann-Liouville theorem). The interactions with the environment are ignored and the considered models are too small to achieve self-averaging [76]. It is unclear at present what would be the characteristic time involved in the thermalization of the translational electronic degrees of freedom of ferromagnetic metals, and how such a thermalization would affect the relation between $\Delta S_z/S_z^0$ and the absorbed energy ΔE. Extensions of our calculations by taking into account a spin-conserving coupling to a bath, which simulates the environment, as well as numerical time propagations of mixed states corresponding to translationally thermalized electronic states are therefore worthwhile.

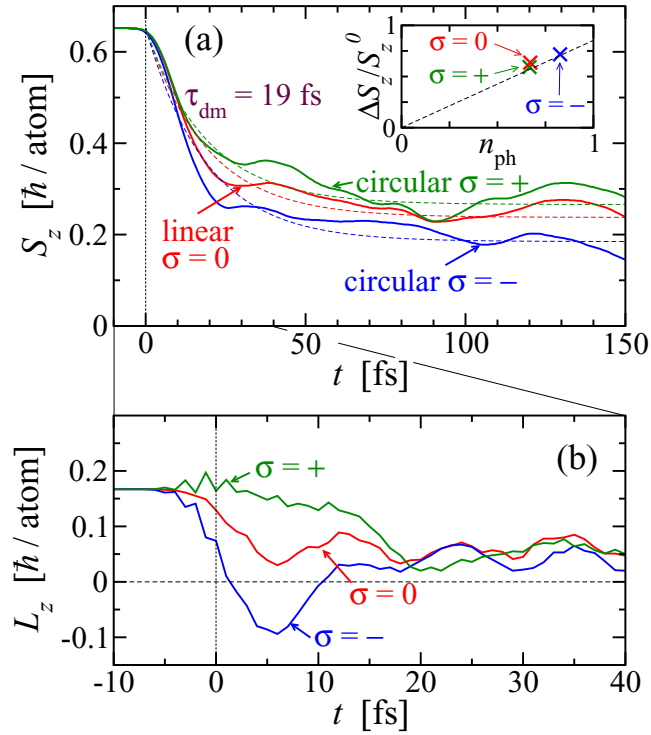

FIG. 5. Time dependence of the average (a) spin moment S_z and (b) orbital moment L_z following the excitation with a $\tau_p = 5$ fs laser pulse having a wave length $\lambda = 1051$ nm and a polarization $\hat{\varepsilon}$ which is in-plane linear ($\sigma = 0$), right circular ($\sigma = +$) or left circular ($\sigma = -$). The full curves are obtained from the exact time evolution of the equilateral triangle model with $N_e = 4$ electrons. The dashed curves in (a) are exponential fits to $S_z(t)$ with a common demagnetization time $\tau_{\rm dm} = 19$ fs. The inset in (a) shows the degree of demagnetization $\Delta S_z/S_z^0$ as a function of the average number of absorbed photons $n_{\rm ph} = \Delta E/\hbar\omega$, together with the same linear approximation (dashed line) as the one found in Fig. 4(b) left.

C. Electric-field polarization

The dependence of the magnetization dynamics on the polarization $\hat{\varepsilon}$ of the incident laser pulse has been investigated by considering linearly and circularly polarized electric fields. Figure 5 shows the time dependence of the spin and orbital angular momenta in an equilateral triangle with $N_e = 4$ electrons. The pumping excitation has a duration $\tau_p = 5$ fs

and a wave length $\lambda = 1051$ nm. Three different electric-field polarizations $\hat{\varepsilon}$ are considered: linear polarization along a NN bond within the xy-plane containing the triangle ($\sigma = 0$), right circular polarization ($\sigma = +$) and left circular polarization ($\sigma = -$). For $\sigma = +$ ($\sigma = -$), the field carries an angular momentum of $\hbar$ ($-\hbar$) which is parallel (antiparallel) to the ground-state spin magnetization S_z^0 along the out-of-plane z direction. Figure 5(a) shows that $S_z(t)$ depends weakly on the considered polarization, in agreement with experiment [77]. In the limit of long times, the spin magnetization decreases to a somewhat larger (smaller) value S_z^∞ after the absorption of a right (left) circular pulse in comparison with the linear pulse. As we shall see, this can be ascribed to the rather small polarization dependence of the absorption cross section. One may also notice that the difference in $S_z(t)$ between left and right polarized light increases at the early stages of the dynamics ($t \lesssim \tau_{\rm dm} = 19$ fs) showing some oscillations for $t \geqslant \tau_{\rm dm}$ [78].

The laser-polarization effects on the orbital magnetic moment L_z are found to be significant only at very short times ($t \lesssim 10$–15 fs). The dynamics of the initially quenched moment $L_z \simeq 0.17\,\hbar$/atom, which is parallel to S_z, is shown in Fig. 5(b) for different laser polarizations. For linear polarization ($\sigma = 0$), the orbital moment decreases to around $L_z \simeq 0.03\,\hbar$/atom during the action of the pulse, while in the case of a left (right) circularly polarized pulse L_z decreases by around $0.26\,\hbar$/atom (increases by around $0.03\,\hbar$/atom) on the same time scale. Notice that for $\sigma = -$, L_z becomes even negative (i.e., antiparallel to S_z) for a very short time. The time lapse during which the polarization dependence of L_z is significant is of the order of the pulse width, in the present case $\tau_p = 5$ fs.

In order to analyze the polarization effects on L_z, let us first notice that the absorption of nonpolarized $\sigma = 0$ pulses consists in electronic dipole transitions mainly from the $3d, m = \pm 1$ orbitals to the $4p, m = 0$ orbitals. Thus, the orbital-moment projection is reduced, which explains qualitatively the laser-induced decrease of L_z observed for linearly polarized pulses [see Fig. 5(b)]. For $\sigma = -$ ($\sigma = +$), L_z is further decreased (enhanced) by around $0.12 - 0.17\,\hbar$/atom in comparison with the $\sigma = 0$ dynamics ($t \lesssim 10$–15 fs). This polarization-dependent decrease (enhancement) is the consequence of the transfer of angular momentum from the laser field to the orbital electronic motion. The left (right) polarized light induces $m \to m - 1$ ($m \to m + 1$) intra-atomic transitions, where the azimuthal quantum number m gives the local contribution to L_z. Neglecting for a moment any spin-orbit transitions and interatomic electron hoppings, this would imply a change $\Delta L_z = \pm\hbar$ in the angular momentum per absorbed photon. Knowing that $n_{\rm ph}/N_a \cong 0.28$ ($n_{\rm ph}/N_a \cong 0.22$) for left (right) polarization, we conclude that the change in L_z induced per absorbed photon explains qualitatively the observed short-time decrease (enhancement) of L_z for $\sigma = -$ ($\sigma = +$). The polarization-dependent change ΔL_z is in fact somewhat smaller than $\pm n_{\rm ph}\hbar/N_a$, since part of the effect is lost due to the rapid interatomic hoppings.

It is also important to remark that the changes in L_z induced by the laser field, and the thus resulting differences in the time dependence of L_z for different polarizations, rapidly vanish once the laser pulse passes. As shown in Fig. 5(b), already 18 fs after the pulse reaches its maximum ($t = 0$) the differences in $L_z(t)$ for different σ are no longer distinguishable from the intrinsic oscillation of $L_z(t)$ due to the dynamics ruled by the field-free $\hat{H}$. The reason behind this is the motion of $3d$ electrons throughout the lattice, which does not conserve the atomic l_{iz}. In TMs d-electron delocalization actually quenches L_z on a very short timescale of the order of $\hbar/t_{ij}^{\alpha\beta} \simeq 1$ fs, where $t_{ij}^{\alpha\beta}$ is the hopping integral between NNs. Thus, the electronic motion tends to wash out any change in the orbital angular momentum, irrespectively of its origin. The results show that the hopping-induced rapid quenching of L_z applies equally well to an enhancement of L_z due to the laser absorption ($\sigma = +$) and to the spin-to-orbital angular momentum transfer due to SOC in the excited states. This explains why the time dependencies of $L_z(t)$ for the different laser polarizations are very similar after the pulse passage. The differences in the excited state for different σ, which are clearly visible in $L_z(t)$ for short times, have only a modest effect on the slower spin dynamics [see Fig. 5(a)]. The latter is actually governed by the spin-to-orbital transfer of angular momentum and the above-mentioned L-quenching electronic motion. As we shall see, the dependence of $S_z(t)$ on the laser polarization is mainly due to the changes in the absorption efficiency for different σ. One concludes that the pd model explains from a microscopic perspective the experimentally observed weak sensitivity of the UFD effect on the laser polarization [77].

In the present calculations, the same fluence $F = 40$ mJ/cm^2 has been used for all electric-field polarizations. The obtained degrees of excitation, as measured by $n_{\rm ph} = \Delta E/\hbar\omega$ and the long-time demagnetization $\Delta S_z/S_z^0$, are quantitatively similar for all σ [see the inset in Fig. 5(a)]. Furthermore, Fig. 5(a) shows that the time dependences of $S_z(t)$ for different σ can all be reasonably well fitted with exponential functions having the same demagnetization time $\tau_{\rm dm} = 19$ fs (dashed curves). Our calculations show no significant effect of the laser polarization $\hat{\varepsilon}$ on $\tau_{\rm dm}$.

In order to investigate the interplay between spin-orbit coupling and laser-ferromagnet interaction, it is interesting to consider pulse durations τ_p that are larger than the timescale of the SOC ($\hbar/|\xi| \simeq 10$ fs) for different laser polarizations. Figure 6 shows the time dependencies of S_z and L_z in an equilateral triangle ($N_e = 4$ electrons) which is excited with a laser pulse having $\tau_p = 20$ fs and $\lambda = 1051$ nm. One observes that $S_z(t)$ and $L_z(t)$ depend significantly on the considered polarization. In the case of L_z, the polarization-dependent changes resulting from direct optical absorption vanish very rapidly as the pulse passes ($t > \tau_p = 20$ fs). As already discussed, this is due to the rapid electron delocalization in the lattice [see Fig. 6(b)]. In contrast, the differences in $S_z(t)$ for the different considered $\hat{\varepsilon}$ remain significant during several hundreds of femtoseconds [see Fig. 6(a)], well beyond the point where the electric field has vanished. The results also show that at long times the circular $\sigma = -$ ($\sigma = +$) pulse induces a more (less) efficient demagnetization $\Delta S_z/S_z^0$ than the linear $\sigma = 0$ pulse. The actual values of $\Delta S_z/S_z^0$ for different $\hat{\varepsilon}$ correlate well with the average number of absorbed photons, as shown in the inset of Fig. 6(a). As for shorter pulses, the demagnetization time $\tau_{\rm dm} = 27$ fs is found to be essentially independent of $\hat{\varepsilon}$.

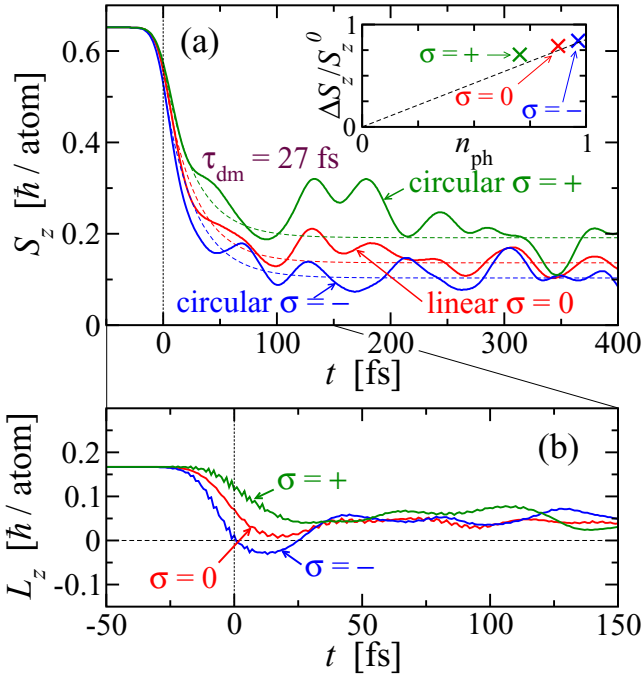

FIG. 6. Time dependence of the average (a) spin moment S_z and (b) orbital moment L_z corresponding to an excitation with a $\tau_p = 20$ fs laser pulse, having a wave length $\lambda = 1051$ nm and a polarization $\hat{\varepsilon}$ which is in-plane linear ($\sigma = 0$), right circular ($\sigma = +$) and left circular ($\sigma = -$). See also the caption of Fig. 5.

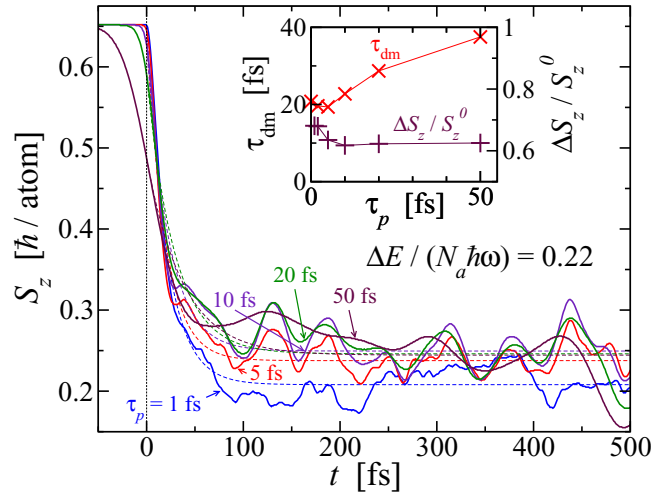

FIG. 7. Time dependence of the average spin moment S_z in an equilateral triangle with $N_e = 4$ electrons resulting from laser-pulse excitations having wave length $\lambda = 1051$ nm and pulse durations $\tau_p = 1$–50 fs. The full curves are obtained from the exact time evolutions, while the dashed curves are the corresponding exponential fits to $S_z(t)$. The laser fluences are such that the average number of absorbed photons per atom is $n_{ph}/N_a = \Delta E/(N_a\hbar\omega) = 0.22$ for all τ_p. The inset shows the demagnetization time τ_{dm} and the long-time demagnetization $\Delta S_z/S_z^0$ as a function of τ_p.

The small polarization dependence of the long-time demagnetization degree $\Delta S_z/S_z^0$ can be interpreted qualitatively in terms of the orbital occupations. Let us first recall that the initial state before the pulse absorption has a small positive orbital moment $L_z \simeq 0.17\,\hbar$ per atom. This means that the $3d$ orbitals with $m > 0$ are in average more likely occupied than the orbitals with $m < 0$. This introduces an asymmetry in the absorption of left and right polarized light (dichroism). Since the orbital polarization of the final $4p$ states is negligible, and the optical matrix elements are invariant upon reversing the circular polarization and the sign of the initial-state m, a higher laser absorption is expected when the average occupation of the dominant initial states is larger. In the case of left (right) circularly polarized light the $m \to m-1$ ($m \to m+1$) selection rule implies that the absorption is dominated by the initial states having $m > 0$ ($m < 0$). Consequently, for $L_z > 0$ the absorption cross section for left-circularly polarized light should be somewhat larger. Our results confirm this trend and can be interpreted accordingly. For example, for a $\tau_p = 5$ fs laser pulse we obtain that the average number of absorbed photons is $n_{ph} = 0.83$ for left-circularly polarized pulses, while it is about $n_{ph} = 0.67$ for linearly or right-circularly polarized pulses. Similarly, for a $\tau_p = 20$ fs laser pulse we obtain $n_{ph} = 0.96$ for left polarization, $n_{ph} = 0.88$ for linear polarization, and $n_{ph} = 0.70$ for right polarization. The insets in Figs. 5 and 6 show the already discussed linear dependence between $\Delta S_z/S_z^0$ and n_{ph}. In fact, the slopes of the straight dashed lines in the insets of Figs. 5(a) and 6(a) are the same as in Fig. 4(b). One concludes that the dependence of $\Delta S_z/S_z^0$ on the laser polarization is mainly a consequence of the different absorption cross sections. It should be, however, noted that the orbital magnetic moments $\langle L_z \rangle$ in TMs are weak. In other words, the differences in the ground-state occupations for positive and negative m are small. Therefore the possibilities of taking advantage of dichroism in order to tune the degree of excitation and $\Delta S_z/S_z^0$ seem quantitatively limited.

D. Pulse duration

The pulse duration τ_p is a central characteristic of the laser excitation whose role on the dynamics deserves to be investigated in some detail. To this aim, exact time propagations have been performed for a triangle having $N_e = 4$ electrons, which is excited with a laser having $\lambda = 1051$ nm and $1\text{fs} \leqslant \tau_p \leqslant 50$ fs. This covers the range from narrow to broad pulses in comparison with the period of oscillation of the field $T = \lambda/c \simeq 3.5$ fs and the SO timescale $\hbar/|\xi| \simeq 10$ fs. Since the radiated energy is directly proportional to the pulse duration τ_p, and the absorption efficiency depends strongly on the frequency distribution of the field, comparing the magnetization dynamics for the same fluence F and different τ_p would be confusing. We have therefore scaled F for each τ_p so that the absorbed energy ΔE and the average number of absorbed photons $n_{ph} = \Delta E/\hbar\omega$ remain constant. In this way, the role of the pulse duration can be effectively assessed. Figure 7 shows the time dependence of the average spin magnetization $S_z(t)$ for $\tau_p = 1$–50 fs and F such that $n_{ph}/N_a = 0.22$. For relatively short pulses ($\tau_p < 10$ fs), the decrease of $S_z(t)$ takes place sharply after the pulse passage. The excitation is sudden, since the electronic system has no time to evolve from a magnetic point of view ($\tau_{dm} \simeq 20$ fs and $\hbar/|\xi| \simeq 10$ fs for $|\xi| = 80$ meV). However, as the pulse

duration is increased, one observes that a significant part of the demagnetization occurs while the laser field is still on. This is particularly clear for $\tau_p = 50$ fs, in which case almost half of the long-time demagnetization has already taken place when the laser pulse reaches its maximum at $t = 0$ (see Fig. 7).

The demagnetization time $\tau_{\rm dm}$ and the degree of demagnetization $\Delta S_z/S_z^0$ are obtained by fitting the exact calculated time dependencies of S_z (full curves) for each τ_p with simple exponential functions. The results, given in the inset of Fig. 7, show that $\Delta S_z/S_z^0 = 0.62$–0.68 is essentially independent of the pulse duration, provided that $n_{\rm ph}$ is kept constant. This holds even for pulse durations which are much longer than the spin-orbit time scale ($\tau_p > \hbar/|\xi| \simeq 10$ fs), which is consistent with the fact that the long-time demagnetization $\Delta S_z/S_z^0$ is controlled primarily by the number of laser-induced single-particle excitations or absorbed photons (see Sec. III B). At least in these examples, the simultaneous action of the laser field and the spin-orbit interactions does not affect the degree of demagnetization at long times. Moreover, no significant interference effects between the laser field and the spin-orbit interactions are seen in $S_z(t)$ and $L_z(t)$.

The inset of Fig. 7 also shows the corresponding demagnetization timescales, which increase from $\tau_{\rm dm} \simeq 20$ fs for very short pulses ($\tau_p \leqslant 5$ fs) to $\tau_{\rm dm} \simeq 38$ fs for $\tau_p = 50$ fs. This trend can be qualitatively understood by recalling that longer pulses imply a narrower spectral distribution $D_\Psi(\epsilon)$ and thus a slower time evolution of the many-body excited state $|\Psi\rangle$. Moreover, in the limit of very short pulses, $\tau_{\rm dm} \simeq 20$ fs remains approximately constant since after a sudden excitation the demagnetization rate is controlled by the SOC. The results confirm that the laser-induced UFD of TMs reflects primarily the intrinsic dynamical behavior of the itinerant-electron many-body system, even in cases where the pulse duration is longer than the characteristic SOC timescale $\hbar/\xi$ and the demagnetization time $\tau_{\rm dm}$.

IV. CONCLUSION

The laser-triggered dynamics of itinerant-electron magnetism has been investigated in the framework of a many-body *pd* Hamiltonian which describes electron delocalization, Coulomb interactions, spin-orbit interactions and the coupling to the laser field on the same footing. The time-dependent many-body state of the system $|\Psi(t)\rangle$ has been exactly calculated by applying a numerical short-time Lanczos propagation method on small cluster models with parameters appropriate for Ni. Starting from the ground state $|\Psi_0\rangle$, the time evolution of $|\Psi(t)\rangle$ has been followed during and after the laser pulse. The relevant observables, in particular the average spin moment $S_z(t)$ and orbital moment $L_z(t)$, have been obtained for a wide range of representative excitation parameters: fluence F, wave length λ, linear and circular polarizations $\hat{\varepsilon}$, and pulse duration τ_p. For all considered excitations, cluster models and band fillings, one observes that $S_z(t)$ decreases rapidly after the pulse passage reaching values close to its long-time limit S_z^∞ in a very short characteristic demagnetization time $\tau_{\rm dm}$ of the order of 20–100 fs. The actual value of $\tau_{\rm dm}$ is found to scale with $1/\xi^2$, where ξ is the spin-orbit coupling strength, which controls the slowest electronic spin-to-orbital angular-momentum transfer. Furthermore, the observed general trends show that whenever the main ingredients of itinerant-electron magnetism are present, namely, band formation, strong intra-atomic $3d$ Coulomb interactions and spin-orbit coupling, the ultrafast demagnetization effect should take place. One concludes that the ultrafast demagnetization of ferromagnetic TMs reflects the intrinsic many-body dynamical behavior of itinerant magnetism. The universality of the effect has been theoretically demonstrated.

The present investigations indicate that ultrafast demagnetization can be regarded as an essentially local process which involves mainly the atomic spin and orbital d-electron degrees of freedom and their immediate local environment. While this justifies small-cluster modelizations, it is also clear that one would like to improve on this limitation by considering larger clusters and extended systems, not least in order to quantify the importance of intermediate- and long-range dynamical effects. Besides the possible consequences on the electronic correlations, improving on the cluster model would allow us to obtain a more quantitative account of the laser absorption efficiency, which has been shown to be crucial for predicting $S_z(t)$. Such improvements will most certainly involve mean-field or functional-integral static approximations of the Coulomb interactions, whose validity could be checked by comparison with the exact results reported in this work. Moreover, our study suggests that the laser-induced ultrafast demagnetization effect, being an essentially local phenomenon, should also take place in ferromagnetic small clusters, nanoparticles and granular systems. It would be therefore most interesting to perform cluster-specific studies of ultrafast demagnetization in order to reveal its size and structural dependence.

Finally, from the fundamental perspective of understanding the underlying physical mechanisms of UFD, it is important to recall that there are other forms of spin-lattice relaxations (e.g., electron-phonon coupling) which have been ignored in the present electronic model and which are expected to contribute to the magnetization dynamics [14,23–29]. It would be therefore very interesting to incorporate these contributions into the present many-body model, in order to quantify their role at the same level as the spin-orbit, Coulomb and hopping electronic effects. In addition, other excitation methods, for instance, involving hot electron injection, mixed thermalized states and indirect optical excitation, should also be investigated in order to challenge the reliability of the present model and the universal character of the ultrafast demagnetization effect.

APPENDIX A: INTERATOMIC HOPPING INTEGRALS

The present Appendix describes the interatomic hopping integrals $t_{jk}^{\alpha\beta}$, which define the single-particle operator $\hat{H}_0$ and its band structure as given by Eq. (2). The matrix elements $t_{jk}^{\alpha\beta}$ are determined by applying the two-center approximation [50], which has found countless successful applications in the description of the electronic structure of solids [79]. Since only the $3d$ and $4p$ valence bands are taken into account in the model, all hopping elements $t_{jk}^{\alpha\beta}$ in $\hat{H}_0$ are obtained in terms of the seven independent Slater-Koster parameters $(dd\sigma)$, $(dd\pi)$, $(dd\delta)$, $(pp\sigma)$, $(pp\pi)$, $(pd\sigma)$, and $(pd\pi)$. The

corresponding expressions for $t_{jk}^{\alpha\beta}$ are [50]

$$
\begin{aligned}
t_{jk}^{4p0,4p0} &= \lambda_z^2(pp\sigma) + \left(1-\lambda_z^2\right)(pp\pi),\\
t_{jk}^{4p0,4p\pm1} &= \mp\lambda_z(\lambda_x \pm i\lambda_y)[(pp\sigma) - (pp\pi)]/\sqrt{2},\\
t_{jk}^{4p\pm1,4p\pm1} &= \left[\left(1-\lambda_z^2\right)(pp\sigma) + \left(1+\lambda_z^2\right)(pp\pi)\right]/2,\\
t_{jk}^{4p+1,4p-1} &= -(\lambda_x - i\lambda_y)^2[(pp\sigma) - (pp\pi)]/2,\\
t_{jk}^{4p0,3d0} &= \lambda_z\left[\left(3\lambda_z^2-1\right)(pd\sigma) + 2\sqrt{3}\left(1-\lambda_z^2\right)(pd\pi)\right]/2,\\
t_{jk}^{4p0,3d\pm1} &= \mp(\lambda_x \pm i\lambda_y)\left[\sqrt{3}\lambda_z^2(pd\sigma) + \left(1-2\lambda_z^2\right)(pd\pi)\right]/\sqrt{2},\\
t_{jk}^{4p0,3d\pm2} &= \lambda_z(\lambda_x \pm i\lambda_y)^2[\sqrt{3}(pd\sigma) - 2(pd\pi)]/\sqrt{8},\\
t_{jk}^{4p\pm1,3d0} &= \mp(\lambda_x \mp i\lambda_y)\left[\left(3\lambda_z^2-1\right)(pd\sigma) - 2\sqrt{3}\lambda_z^2(pd\pi)\right]/\sqrt{8},\\
t_{jk}^{4p\pm1,3d\pm1} &= \lambda_z\left[\sqrt{3}\left(1-\lambda_z^2\right)(pd\sigma) + 2\lambda_z^2(pd\pi)\right]/2,\\
t_{jk}^{4p\pm1,3d\pm2} &= \mp(\lambda_x \pm i\lambda_y)\left[\sqrt{3}\left(1-\lambda_z^2\right)(pd\sigma) + 2\left(1+\lambda_z^2\right)(pd\pi)\right]/4,\\
t_{jk}^{4p\pm1,3d\mp1} &= -\lambda_z(\lambda_x \mp i\lambda_y)^2[\sqrt{3}(pd\sigma) - 2(pd\pi)]/2,\\
t_{jk}^{4p\pm1,3d\mp2} &= \mp(\lambda_x \mp i\lambda_y)^3[\sqrt{3}(pd\sigma) - 2(pd\pi)]/4,\\
t_{jk}^{3d0,3d0} &= \left(3\lambda_z^2-1\right)^2(dd\sigma)/4 + 3\lambda_z^2\left(1-\lambda_z^2\right)(dd\pi) + 3\left(1-\lambda_z^2\right)^2(dd\delta)/4,\\
t_{jk}^{3d0,3d\pm1} &= \mp\lambda_z\sqrt{3}(\lambda_x \pm i\lambda_y)\left[\left(3\lambda_z^2-1\right)(dd\sigma) + 2\left(1-2\lambda_z^2\right)(dd\pi) - \left(1-\lambda_z^2\right)(dd\delta)\right]/\sqrt{8},\\
t_{jk}^{3d0,3d\pm2} &= \sqrt{3}(\lambda_x \pm i\lambda_y)^2\left[\left(3\lambda_z^2-1\right)(dd\sigma) - 4\lambda_z^2(dd\pi) + \left(1+\lambda_z^2\right)(dd\delta)\right]/\sqrt{32},\\
t_{jk}^{3d\pm1,3d\pm1} &= \left[3\lambda_z^2\left(1-\lambda_z^2\right)(d,d;\sigma) + \left(4\lambda_z^4 - 3\lambda_z^2 + 1\right)(dd\pi) + \left(1-\lambda_z^4\right)(dd\delta)\right]/2,\\
t_{jk}^{3d\pm1,3d\pm2} &= \mp\lambda_z(\lambda_x \pm i\lambda_y)\left[3\left(1-\lambda_z^2\right)(dd\sigma) + 4\lambda_z^2(dd\pi) - \left(3+\lambda_z^2\right)(dd\delta)\right]/4,\\
t_{jk}^{3d+1,3d-1} &= -(\lambda_x - i\lambda_y)^2\left[3\lambda_z^2(dd\sigma) + \left(1-4\lambda_z^2\right)(dd\pi) + \left(\lambda_z^2-1\right)(dd\delta)\right]/2,\\
t_{jk}^{3d\pm1,3d\mp2} &= \mp\lambda_z(\lambda_x \mp i\lambda_y)^3[3(dd\sigma) - 4(dd\pi) + (dd\delta)]/4,\\
t_{jk}^{3d\pm2,3d\pm2} &= \left[3\left(1-\lambda_z^2\right)^2(dd\sigma) + 4\left(1-\lambda_z^4\right)(dd\pi) + \left(\lambda_z^4 + 6\lambda_z^2 + 1\right)(dd\delta)\right]/8, \quad \text{and}\\
t_{jk}^{3d+2,3d-2} &= (\lambda_x - i\lambda_y)^4[3\,(dd\sigma) - 4(dd\pi) + (dd\delta)]/8,
\end{aligned}
\tag{A1}
$$

where $\hat{z}$ has been chosen as the m-quantization axis, and $\lambda_\mu = \vec{R}_{jk}\cdot\hat{\mu}/R_{jk}$ denotes the direction cosine of the interatomic vector $\vec{R}_{jk} = \vec{R}_j - \vec{R}_k$ ($\hat{\mu} = \hat{x}$, $\hat{y}$ or $\hat{z}$). Notice that the hopping elements which are not explicitly given can be obtained by applying the relation $t_{jk}^{\alpha\beta} = t^{\alpha\beta}(\vec{R}_{jk}) = [t^{\beta\alpha}(-\vec{R}_{jk})]^*$. Further details may be found in Ref. [50].

As described in Sec. II, the *pd* model has been simplified in order to keep the dimension of the many-body Hilbert space and the numerical effort involved in the exact time evolution tractable. Thus the $3d$ orbitals are approximated by three degenerate levels having $|m| \leqslant 1$ and the $4p$ orbitals by a single level having $m = 0$. This reduction of the number of bands implies that only the four Slater-Koster parameters $(dd\sigma)$, $(dd\pi)$, $(pp\sigma)$, and $(pd\sigma)$ are necessary in order to determine all hopping integrals $t_{jk}^{\alpha\beta}$. The corresponding expressions for $t_{jk}^{\alpha\beta}$ are

$$
\begin{aligned}
t_{jk}^{4p0,4p0} &= (pp\sigma),\\
t_{jk}^{4p0,3d0} &= \lambda_z(pd\sigma),\\
t_{jk}^{4p0,3d\pm1} &= \mp(\lambda_x \pm i\lambda_y)(pd\sigma)/\sqrt{2},\\
t_{jk}^{3d0,3d0} &= \lambda_z^2(dd\sigma) + \left(1-\lambda_z^2\right)(dd\pi),\\
t_{jk}^{3d0,3d\pm1} &= \mp\lambda_z(\lambda_x \pm i\lambda_y)[(dd\sigma) - (dd\pi)]/\sqrt{2},\\
t_{jk}^{3d\pm1,3d\pm1} &= \left[\left(1-\lambda_z^2\right)(dd\sigma) + \left(1+\lambda_z^2\right)(dd\pi)\right]/2, \quad \text{and}\\
t_{jk}^{3d+1,3d-1} &= -(\lambda_x - i\lambda_y)^2[(dd\sigma) - (dd\pi)]/2.
\end{aligned}
\tag{A2}
$$

The values of the Slater-Koster parameters are given in the main text.

APPENDIX B: ELECTRIC DIPOLE MATRIX ELEMENTS

The dominant intra-atomic dipole matrix elements $\langle\alpha|\vec{r}|\beta\rangle$ characterizing the interaction $\hat{H}_E$ with the laser field [see Eqs. (7) and (8)] can be expressed in terms of the irreducible spherical tensor operator $\hat{T}^{(k)}_q$ of rank $k = 1$ and components q given by

$$\begin{aligned}\hat{T}^{(1)}_{+1} &= -\frac{1}{\sqrt{2}}(\hat{x} + i\hat{y}),\\ \hat{T}^{(1)}_{-1} &= \frac{1}{\sqrt{2}}(\hat{x} - i\hat{y}),\\ \hat{T}^{(1)}_{0} &= \hat{z}.\end{aligned} \tag{B1}$$

The elements of $\hat{T}^{(1)}_q$ between the atomic orbitals $|nlm\rangle$ having principal quantum number n, orbital angular momentum l and z-axis projection m are given by the Wigner-Eckart relation [80]

$$\langle nlm|\hat{T}^{(k)}_q|n'l'm'\rangle = \langle l'k; m'q|lm\rangle \frac{\langle nl||\hat{T}^{(k)}||n'l'\rangle}{\sqrt{2l'+1}}, \tag{B2}$$

where $\langle nl||\hat{T}^{(k)}||n'l'\rangle$ is the reduced matrix element and the scalar products $\langle l'k; m'q|lm\rangle$ are the Clebsch-Gordan coefficients. Thus the matrix element $\langle nlm|\hat{T}^{(k)}_q|n'l'm'\rangle$ in Eq. (B2) can be interpreted as a projection resulting from the addition of the angular momenta $\vec{l}'$ and $\vec{k}$ to $\vec{l}$ ($\vec{l}' \oplus \vec{k} = \vec{l}$). Since $\langle nl||\hat{T}^{(1)}||n'l'\rangle$ is independent of m', q, and m, all the dipole matrix elements entering $\hat{H}_E$ are characterized by a single parameter $\langle 3d||\hat{T}^{(1)}||4p\rangle$, the dependence on m, m' and q being given by the known Clebsch-Gordan coefficients. Since the operator $\hat{H}_E$ is given by a product of $\hat{\vec{r}}$ and $\vec{E}$, the matrix element $\langle 3d||\hat{T}^{(1)}||4p\rangle$ gives a measure of the strength of the coupling between the electronic translational degrees of freedom and the external electric field $\vec{E}$ [see Eqs. (7) and (8) of the main text].

The nonvanishing dipole matrix elements then read

$$\begin{aligned}\langle 3dm|\hat{x}|4pm'\rangle &= (\delta_{m,m'-1} - \delta_{m,m'+1})(\sqrt{|m|/12} + \delta_{m,0}/6)\\ &\quad\times \langle 3d||\hat{T}^{(1)}||4p\rangle,\\ \langle 3dm|\hat{y}|4pm'\rangle &= i(\delta_{m,m'-1} + \delta_{m,m'+1})(\sqrt{|m|/12} + \delta_{m,0}/6)\\ &\quad\times \langle 3d||\hat{T}^{(1)}||4p\rangle,\\ \langle 3dm|\hat{z}|4pm'\rangle &= \delta_{m,m'}(|m|/\sqrt{6} + \delta_{m,0}\sqrt{2/9})\langle 3d||\hat{T}^{(1)}||4p\rangle.\end{aligned} \tag{B3}$$

In the case of circular polarization $\hat{\varepsilon}_\pm$, the relevant matrix elements are

$$\begin{aligned}\langle 4pm'|\hat{\varepsilon}_\pm \cdot \hat{\vec{r}}|3dm\rangle &= \pm\delta_{m',m\pm1}(\sqrt{|m|/6} + \sqrt{2}\delta_{m,0}/6)\\ &\quad\times \langle 3d||\hat{T}^{(1)}||4p\rangle^*.\end{aligned} \tag{B4}$$

Taking into account the reduction of the local orbital degeneracy introduced in Sec. II, the nonvanishing electric-dipole matrix elements are simplified as follows. For linear electric-field polarization, they read

$$\begin{aligned}\langle 3dm|\hat{x}|4p0\rangle &= -m\langle 3d||\hat{T}^{(1)}||4p\rangle/\sqrt{2},\\ \langle 3dm|\hat{y}|4p0\rangle &= i(1-\delta_{m,0})\langle 3d||\hat{T}^{(1)}||4p\rangle/\sqrt{2},\\ \langle 3dm|\hat{z}|4p0\rangle &= \delta_{m,0}\langle 3d||\hat{T}^{(1)}||4p\rangle,\end{aligned} \tag{B5}$$

while for circular polarization they are given by

$$\langle 4p0|\hat{\varepsilon}_\pm \cdot \hat{\vec{r}}|3dm\rangle = \pm\delta_{m,\mp1}\langle 3d||\hat{T}^{(1)}||4p\rangle^*. \tag{B6}$$

The value of $\langle 3d||\hat{T}^{(1)}||4p\rangle$ is given in the main text.

[1] E. Beaurepaire, J.-C. Merle, A. Daunois, and J.-Y. Bigot, Phys. Rev. Lett. **76**, 4250 (1996).

[2] J. Hohlfeld, E. Matthias, R. Knorren, and K. H. Bennemann, Phys. Rev. Lett. **78**, 4861 (1997).

[3] B. Koopmans, M. van Kampen, J. T. Kohlhepp, and W. J. M. de Jonge, Phys. Rev. Lett. **85**, 844 (2000).

[4] M. Lisowski, P. A. Loukakos, A. Melnikov, I. Radu, L. Ungureanu, M. Wolf, and U. Bovensiepen, Phys. Rev. Lett. **95**, 137402 (2005).

[5] M. Cinchetti, M. Sánchez Albaneda, D. Hoffmann, T. Roth, J.-P. Wüstenberg, M. Krauß, O. Andreyev, H. C. Schneider, M. Bauer, and M. Aeschlimann, Phys. Rev. Lett. **97**, 177201 (2006).

[6] A. Melnikov, H. Prima-Garcia, M. Lisowski, T. Gießel, R. Weber, R. Schmidt, C. Gahl, N. M. Bulgakova, U. Bovensiepen, and M. Weinelt, Phys. Rev. Lett. **100**, 107202 (2008).

[7] M. Wietstruk, A. Melnikov, C. Stamm, T. Kachel, N. Pontius, M. Sultan, C. Gahl, M. Weinelt, H. A. Dürr, and U. Bovensiepen, Phys. Rev. Lett. **106**, 127401 (2011).

[8] P. Tengdin, W. You, C. Chen, X. Shi, D. Zusin, Y. Zhang, C. Gentry, A. Blonsky, M. Keller, P. M. Oppeneer, H. C. Kapteyn, Z. Tao, and M. M. Murnane, Sci. Adv. **4**, eaap9744 (2018).

[9] H.-S. Rhie, H. A. Dürr, and W. Eberhardt, Phys. Rev. Lett. **90**, 247201 (2003).

[10] C. Stamm, T. Kachel, N. Pontius, R. Mitzner, T. Quast, K. Holldack, S. Khan, C. Lupulescu, E. F. Aziz, M. Wietstruk, H. A. Dürr, and W. Eberhardt, Nat. Mater. **6**, 740 (2007).

[11] C. Stamm, N. Pontius, T. Kachel, M. Wietstruk, and H. A. Dürr, Phys. Rev. B **81**, 104425 (2010).

[12] R. Gort, K. Bühlmann, S. Däster, G. Salvatella, N. Hartmann, Y. Zemp, S. Holenstein, C. Stieger, A. Fognini, T. U. Michlmayr, T. Bähler, A. Vaterlaus, and Y. Acremann, Phys. Rev. Lett. **121**, 087206 (2018).

[13] E. Carpene, E. Mancini, C. Dallera, M. Brenna, E. Puppin, and S. De Silvestri, Phys. Rev. B **78**, 174422 (2008).

[14] B. Koopmans, G. Malinowski, F. Dalla Longa, D. Steiauf, M. Fähnle, T. Roth, M. Cinchetti, and M. Aeschlimann, Nat. Mater. **9**, 259 (2010).

[15] E. Carpene, H. Hedayat, F. Boschini, and C. Dallera, Phys. Rev. B **91**, 174414 (2015).

[16] S. Eich, M. Plötzing, M. Rollinger, S. Emmerich, R. Adam, C. Chen, H. C. Kapteyn, M. M. Murnane, L. Plucinski, D. Steil, B. Stadtmüller, M. Cinchetti, M. Aeschlimann, C. M. Schneider, and S. Mathias, Sci. Adv. **3**, e1602094 (2017).

[17] N. Kazantseva, D. Hinzke, U. Nowak, R. W. Chantrell, and O. Chubykalo-Fesenko, Phys. Status Solidi B **244**, 4389 (2007).

[18] U. Atxitia, O. Chubykalo-Fesenko, N. Kazantseva, D. Hinzke, U. Nowak, and R. W. Chantrell, Appl. Phys. Lett. **91**, 232507 (2007).

[19] M. Krauß, T. Roth, S. Alebrand, D. Steil, M. Cinchetti, M. Aeschlimann, and H. C. Schneider, Phys. Rev. B **80**, 180407(R) (2009).

[20] A. B. Schmidt, M. Pickel, M. Donath, P. Buczek, A. Ernst, V. P. Zhukov, P. M. Echenique, L. M. Sandratskii, E. V. Chulkov, and M. Weinelt, Phys. Rev. Lett. **105**, 197401 (2010).

[21] B. Y. Mueller and B. Rethfeld, Phys. Rev. B **90**, 144420 (2014).

[22] K. Leckron, S. Vollmar, and H. C. Schneider, Phys. Rev. B **96**, 140408(R) (2017).

[23] B. Koopmans, H. H. J. E. Kicken, M. van Kampen, and W. J. M. de Jonge, J. Magn. Magn. Mater. **286**, 271 (2005).

[24] B. Koopmans, J. J. M. Ruigrok, F. Dalla Longa, and W. J. M. de Jonge, Phys. Rev. Lett. **95**, 267207 (2005).

[25] D. Steiauf and M. Fähnle, Phys. Rev. B **79**, 140401(R) (2009).

[26] D. Steiauf, C. Illg, and M. Fähnle, J. Magn. Magn. Mater. **322**, L5 (2010).

[27] M. Fähnle and C. Illg, J. Phys.: Condens. Matter **23**, 493201 (2011).

[28] K. Carva, M. Battiato, and P. M. Oppeneer, Phys. Rev. Lett. **107**, 207201 (2011).

[29] B. Y. Mueller, A. Baral, S. Vollmar, M. Cinchetti, M. Aeschlimann, H. C. Schneider, and B. Rethfeld, Phys. Rev. Lett. **111**, 167204 (2013).

[30] M. Battiato, K. Carva, and P. M. Oppeneer, Phys. Rev. Lett. **105**, 027203 (2010).

[31] A. Melnikov, I. Razdolski, T. O. Wehling, E. Th. Papaioannou, V. Roddatis, P. Fumagalli, O. Aktsipetrov, A. I. Lichtenstein, and U. Bovensiepen, Phys. Rev. Lett. **107**, 076601 (2011).

[32] M. Battiato, K. Carva, and P. M. Oppeneer, Phys. Rev. B **86**, 024404 (2012).

[33] D. Rudolf, C. La-O-Vorakiat, M. Battiato, R. Adam, J. M. Shaw, E. Turgut, P. Maldonado, S. Mathias, P. Grychtol, H. T. Nembach, T. J. Silva, M. Aeschlimann, H. C. Kapteyn, M. M. Murnane, C. M. Schneider, and P. M. Oppeneer, Nat. Commun. **3**, 1037 (2012).

[34] A. Eschenlohr, M. Battiato, P. Maldonado, N. Pontius, T. Kachel, K. Holldack, R. Mitzner, A. Föhlisch, P. M. Oppeneer, and C. Stamm, Nat. Mater. **12**, 332 (2013).

[35] E. Turgut, C. La-O-vorakiat, J. M. Shaw, P. Grychtol, H. T. Nembach, D. Rudolf, R. Adam, M. Aeschlimann, C. M. Schneider, T. J. Silva, M. M. Murnane, H. C. Kapteyn, and S. Mathias, Phys. Rev. Lett. **110**, 197201 (2013).

[36] A. J. Schellekens, W. Verhoeven, T. N. Vader, and B. Koopmans, Appl. Phys. Lett. **102**, 252408 (2013).

[37] J. K. Dewhurst, P. Elliott, S. Shallcross, E. K. U. Gross, and S. Sharma, Nano Lett. **18**, 1842 (2018).

[38] G. P. Zhang and W. Hübner, Phys. Rev. Lett. **85**, 3025 (2000).

[39] J.-Y. Bigot, M. Vomir, and E. Beaurepaire, Nat. Phys. **5**, 515 (2009).

[40] H. Vonesch and J.-Y. Bigot, Phys. Rev. B **85**, 180407(R) (2012).

[41] K. Krieger, J. K. Dewhurst, P. Elliott, S. Sharma, and E. K. U. Gross, J. Chem. Theory Comput. **11**, 4870 (2015).

[42] P. Elliott, K. Krieger, J. K. Dewhurst, S. Sharma, and E. K. U. Gross, New J. Phys. **18**, 013014 (2016).

[43] K. Krieger, P. Elliott, T. Müller, N. Singh, J. K. Dewhurst, E. K. U. Gross, and S. Sharma, J. Phys.: Condens. Matter **29**, 224001 (2017).

[44] V. Shokeen, M. Sanchez Piaia, J.-Y. Bigot, T. Müller, P. Elliott, J. K. Dewhurst, S. Sharma, and E. K. U. Gross, Phys. Rev. Lett. **119**, 107203 (2017).

[45] W. Töws and G. M. Pastor, Phys. Rev. Lett. **115**, 217204 (2015).

[46] A. R. Khorsand, M. Savoini, A. Kirilyuk, A. V. Kimel, A. Tsukamoto, A. Itoh, and Th. Rasing, Phys. Rev. Lett. **108**, 127205 (2012).

[47] T. A. Ostler, J. Barker, R. F. L. Evans, R. W. Chantrell, U. Atxitia, O. Chubykalo-Fesenko, S. El Moussaoui, L. Le Guyader, E. Mengotti, L. J. Heyderman, F. Nolting, A. Tsukamoto, A. Itoh, D. Afanasiev, B. A. Ivanov, A. M. Kalashnikova, K. Vahaplar, J. Mentink, A. Kirilyuk, Th. Rasing, and A. V. Kimel, Nat. Commun. **3**, 666 (2012).

[48] U. Bierbrauer, S. T. Weber, D. Schummer, M. Barkowski, A.-K. Mahro, S. Mathias, H. C. Schneider, B. Stadtmüller, M. Aeschlimann, and B. Rethfeld, J. Phys.: Condens. Matter **29**, 244002 (2017).

[49] M. Born and J. R. Oppenheimer, Ann. Phys. **389**, 457 (1927).

[50] J. C. Slater and G. F. Koster, Phys. Rev. **94**, 1498 (1954).

[51] G. Nicolas, J. Dorantes-Dávila, and G. M. Pastor, Phys. Rev. B **74**, 014415 (2006).

[52] R. Garibay-Alonso, J. Dorantes-Dávila, and G. M. Pastor, Phys. Rev. B **91**, 184408 (2015).

[53] T. Uchida and Y. Kakehashi, Phys. Rev. B **64**, 054402 (2001).

[54] Y. Kakehashi, T. Shimabukuro, T. Tamashiro, and T. Nakamura, J. Phys. Soc. Jpn. **77**, 094706 (2008).

[55] Y. Kakehashi and M. A. R. Patoary, Phys. Rev. B **83**, 144409 (2011).

[56] See, for instance, Refs. [52,53,55], as well as references therein.

[57] J. Hubbard, Proc. R. Soc. London A **276**, 238 (1963).

[58] J. Kanamori, Prog. Theor. Phys. **30**, 275 (1963).

[59] M. C. Gutzwiller, Phys. Rev. Lett. **10**, 159 (1963).

[60] D. A. Papaconstantopoulos, *Handbook of the Band Structure of Elemental Solids* (Plenum Press, New York, 1986).

[61] R. H. Victora, L. M. Falicov, and S. Ishida, Phys. Rev. B **30**, 3896 (1984); R. H. Victora and L. M. Falicov, *ibid.* **31**, 7335 (1985).

[62] O. K. Andersen, W. Klose, and H. Nohl, Phys. Rev. B **17**, 1209 (1978).

[63] D. G. Pettifor, J. Phys. F: Met. Phys. **7**, 613 (1977).

[64] S. Hüfner and G. K. Wertheim, Phys. Lett. A **51**, 299 (1975).

[65] W. Eberhardt and E. W. Plummer, Phys. Rev. B **21**, 3245 (1980).

[66] L. A. Feldkamp and L. C. Davis, Phys. Rev. B **22**, 3644 (1980).

[67] R. H. Victora and L. M. Falicov, Phys. Rev. Lett. **55**, 1140 (1985).

[68] P. Bruno, *Magnetismus von Festkörpern und Grenzflächen* (KFA, Jülich, 1993), Chap. 24.

[69] L. D. Landau and E. M. Lifshitz, *Quantum Mechanics: Non-relativistic Theory* (Elsevier Butterworth-Heinemann, Oxford, 1981).

[70] D. J. Tannor, *Introduction to Quantum Mechanics: A time-Dependent Perspective* (University Science Books, Sausalito, California, 2007).

[71] J. J. Sakurai, *Modern Quantum Mechanics* (Addison-Wesley, Reading, Massachusetts, 1994).

[72] G. M. Pastor, J. Dorantes-Dávila, S. Pick, and H. Dreyssé, Phys. Rev. Lett. **75**, 326 (1995).

[73] J. Dorantes-Dávila and G. M. Pastor, Phys. Rev. Lett. **81**, 208 (1998).

[74] J. L. Rodríguez-López, J. Dorantes-Dávila, and G. M. Pastor, Phys. Rev. B **57**, 1040 (1998).

[75] R. A. Guirado-López, J. Dorantes-Dávila, and G. M. Pastor, Phys. Rev. Lett. **90**, 226402 (2003).

[76] J. M. Deutsch, Phys. Rev. A **43**, 2046 (1991).

[77] F. Dalla Longa, J. T. Kohlhepp, W. J. M. de Jonge, and B. Koopmans, Phys. Rev. B **75**, 224431 (2007).

[78] In addition, other different linear electric field polarizations $\hat{\varepsilon}$ have also been considered. For all $\hat{\varepsilon}$ within the triangle plane the optical absorptions and subsequent dynamics have been found to be quantitatively very similar. However, for $\hat{\varepsilon}$ normal to the triangle plane ($\hat{\varepsilon} = \hat{z}$) we obtain a strong reduction of the optical absorption. Thus, for a given F, the demagnetization strength is significantly smaller than in the case of in-plane polarizations.

[79] W. A. Harrison, *Electronic Structure and the Properties of Solids* (Dover Pubn Inc, Dover, 1989).

[80] A. Messiah, *Quantum Mechanics* (Elsevier Science B. V., Amsterdam, 1981), Vol. II.